Physics – Uspekhi **57** (12) 1199 – 1228 (2014)

PHYSICS OF OUR DAYS

PACS numbers: **07.87.+v**, **95.55.–n**, **97.10.–q**, **98.62.–g**, **98.80.–k**

Review of scientific topics for the Millimetron space observatory

N S Kardashev, I D Novikov, V N Lukash, S V Pilipenko, E V Mikheeva, D V Bisikalo, D S Wiebe, A G Doroshkevich, A V Zasov, I I Zinchenko, P B Ivanov, V I Kostenko, T I Larchenkova, S F Likhachev, I F Malov, V M Malofeev, A S Pozanenko, A V Smirnov, A M Sobolev, A M Cherepashchuk, Yu A Shchekinov

DOI: 10.3367/UFNe.0184.201412c.1319

Contents

1. Introduction **1200**

2. Interstellar medium and star formation regions in the Galaxy **1202**

2.1 Structure and kinematics of the interstellar medium; 2.2 Star formation regions in the Galaxy; 2.3 Protoplanetary discs and protostellar objects; 2.4 Maser sources

3. Stars and planets **1207**

3.1 Direct observations of exoplanets; 3.2 Mass loss at late stages of stellar evolutions; 3.3 Search for extraterrestrial life

4. Supernovae and supernova remnants **1209**

4.1 White dwarfs; 4.2 Pulsar radio emission; 4.3 Relativistic objects in the centers of globular clusters; 4.4 Origin of ultraluminous X-ray sources; 4.5. Supernovae

5. Black holes and jets **1213**

5.1 Nearby black holes; 5.2 Shadows of black holes; 5.3 Remote black holes; 5.4 Physics of jets; 5.5 Jets from cosmic gamma-ray bursts

6. Galaxies **1216**

6.1 Evolution of galaxies; 6.2 Regions with low star-formation rate; 6.3 Extragalactic star-formation regions; 6.4 Dynamics of the interstellar medium and chemical evolution of Universe; 6.5 Gravitational lensing at high redshifts

7. Cosmology **1222**

7.1 Infrared background and galaxy surveys; 7.2 Cosmological angular distances; 7.3 Distant galaxies and reionization of the Universe; 7.4 Galaxy clusters; 7.5 Gamma-ray burst afterglows and host galaxies; 7.6 Primordial black and white holes, wormholes, and the Multiverse

8. Conclusion **1225**

References **1226**

N S Kardashev, V N Lukash, S V Pilipenko, E V Mikheeva, A G Doroshkevich, P B Ivanov, V I Kostenko, T I Larchenkova, S F Likhachev, A V Smirnov Astro Space Center, Lebedev Physical Institute, Russian Academy of Sciences,
ul. Profsoyuznaya 84/32, 117997 Moscow, Russian Federation
E-mail: nkardash@asc.rssi.ru, lukash@asc.rssi.ru, spilipenko@asc.rssi.ru, helen@asc.rssi.ru, dorr@asc.rssi.ru, pbi20@cam.ac.uk, vkostenko@asc.rssi.ru ltanya@asc.rssi.ru, slikhach@asc.rssi.ru, asmirn@asc.rssi.ru

I D Novikov Astro Space Center, Lebedev Physical Institute, Russian Academy of Sciences,
ul. Profsoyuznaya 84/32, 117997 Moscow, Russian Federation
E-mail: novikov@asc.rssi.ru
Niels Bohr International Academy, Niels Bohr Institute, Blegdamsvej 17, DK-2100 Copenhagen, Denmark

D V Bisikalo, D S Wiebe Institute of Astronomy, Russian Academy of Sciences,
ul. Pyatnitskaya 48, 119017 Moscow, Russian Federation
E-mail: bisikalo@inasan.ru, dwiebe@inasan.ru

A V Zasov, A M Cherepashchuk Sternberg State Astronomical Institute, Faculty of Physics, Moscow State University,
Universitetskii prosp. 13, 119991 Moscow, Russian Federation
E-mail: zasov@sai.msu.ru, cher@sai.msu.ru

I I Zinchenko Institute of Applied Physics, Russian Academy of Sciences,
ul. Ul'yanova 46, 603950 Nizhnii Novgorod, Russian Federation;
Lobachevskii Nizhnii Novgorod State University,
prosp. Gagarina 23, 603950 Nizhnii Novgorod, Russian Federation
E-mail: zin@appl.sci-nnov.ru

I F Malov, V M Malofeev Astro Space Center, Lebedev Physical Institute, Russian Academy of Sciences, Pushchino Radio Astronomy Observatory,
142290 Pushchino, Moscow Region, Russian Federation
E-mail: malov@prao.ru, malofeev@prao.ru

A S Pozanenko Space Research Institute, Russian Academy of Sciences,
ul. Profsoyuznaya 84/32, 117997 Moscow, Russian Federation
E-mail: apozanen@iki.rssi.ru

A M Sobolev Ural Federal University, Institute of Natural Sciences, Astronomical Observatory,
prosp. Lenina 51, 620000 Ekaterinburg, Russian Federation
E-mail: Andrej.Sobolev@urfu.ru

Yu A Shchekinov Southern Federal University,
ul. Bol'shaya Sadovaya 105/42, 344006 Rostov-on-Don, Russian Federation
E-mail: yus@sfedu.ru

Received 31 July 2014
Uspekhi Fizicheskikh Nauk **184** (12) 1319 – 1352 (2014)
DOI: 10.3367/UFNr.0184.201412c.1319
Translated by K A Postnov; edited by A M Semikhatov

Abstract. This paper reviews a wide range of questions in astrophysics and cosmology that can be answered by astronomical observations in the far-IR to millimeter wavelength range and which include the formation and evolution of stars and planets, galaxies, and the interstellar medium, the study of black holes, and the development of the cosmological model. These questions are considered in relation to the Millimetron Space Observatory (Spectrum-M project), which is equipped with a 10 m aperture cooled telescope and can operate both as a single-dish telescope and as part of a space–ground very long baseline interferometer.

1. Introduction

The Millimetron space observatory is aimed at conducting astronomical observations to probe a broad range of objects in the Universe in the wavelength range 20 μm to 20 mm. Since the early 1990s, there has been a growing interest in astrophysical and cosmological studies in this range, which is very important for different types of astronomical observations, including the continuum and spectral line studies, polarimetry, and variations of different parameters.

The millimeter ($1\text{ mm} < \lambda < 1\text{ cm}$), submillimeter ($0.1 < \lambda < 1\text{ mm}$), and far infrared (FIR) ($50 < \lambda < 300$ μm) bands are unique for astronomy for the following reasons:

• the maximum of the cosmic microwave background (CMB) is at a wavelength of 1 mm. This is the electromagnetic emission that survived from the very early stages of the Universe (the Big Bang) and fills space almost homogeneously. A detailed study of the spatial structure, spectrum, and polarization of the CMB will help in solving fundamental issues in astrophysics and cosmology, including the development of the standard cosmological model, the formation and evolution of the first objects in the Universe, and the determination of the parameters of dark matter and dark energy;

• the maximum of the emission that comes from the coldest objects in the Universe, including gas and dust clouds in our and other galaxies, asteroids, comets, and planets, is in the FIR. Therefore, observations in this range allow the exploration of the interstellar medium evolution in the process of gravitational contraction leading to the formation of stars and planetary systems, and ultimately to the appearance of life and civilization;

• the natural sky background emission reaches a minimum near 300 μm. This background is the sum of contributions from different sources along the line of sight and the CMB (Fig. 1a). Observations in this range will enable probing very faint astronomical objects — galaxies, stars, black holes, exoplanets, etc. — with a record high sensitivity;

• there are many atomic and molecular spectral lines located in the submillimeter and FIR ranges, allowing the determination of the chemical composition and physical properties of gas in different objects ranging from protoplanetary discs to galaxies at different epochs;

• observations in the submillimeter range can significantly increase the angular resolution by using very long baseline interferometry (VLBI), which is necessary to study the most compact objects, such as the surroundings of black holes, some pulsars, and gamma-ray bursts;

• the medium surrounding many interesting astronomical objects is most transparent in these wavelength ranges compared with the neighboring spectral bands, both at short wavelengths (due to interstellar dust absorption) and at long wavelengths (due to synchrotron self-absorption, thermal plasma absorption, and scattering on plasma inhomogeneities).

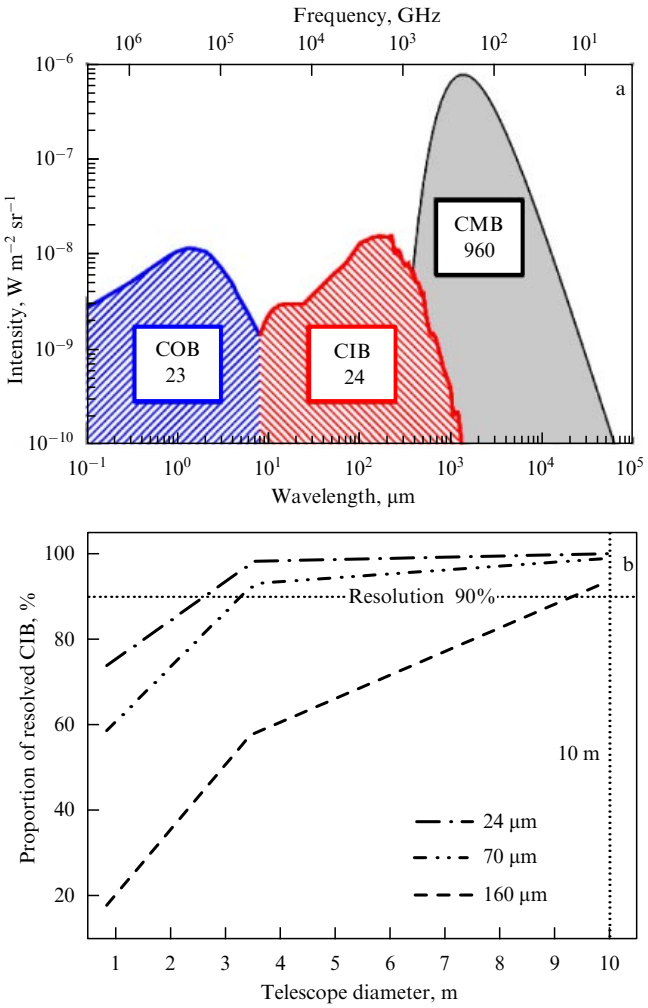

Figure 1. (a) Extragalactic background spectrum. COB — cosmic optical background, CIB — cosmic infrared background, CMB — cosmic microwave background. Numbers show the total intensity of the background components in units nW m^{-2} sr^{-1} [1]. (b) The possible proportion of the CIB resolved into individual sources as a function of the telescope diameter for several wavelengths.

One of the largest single ground-based telescopes especially designed for submillimeter observations is the James Clerk Maxwell Telescope (JCMT) (http://www.jach.hawaii.edu/JCMT/) with a 15 m aperture, located near Mauna Kea (Hawaii) at an altitude of more than 4000 m above sea level. Heterodyne receivers at the JCMT cover all transparency windows of Earth's atmosphere in the 200–700 GHz frequency band, and the bolometric receiver based on an array detector (10,240 elements) operates at two wavelengths, 450 and 850 μm. The JCMT is used to study the Solar System, interstellar gas and dust, as well as distant galaxies. Using the JCMT, submillimeter galaxies have been discovered because submillimeter emission dominates over the optical emission.

The Atacama Large Millimeter/submillimeter Array (ALMA) is the most promising ground-based submillimeter instrument (http://www.almaobservatory.org), which is now at the commissioning phase. ALMA is a compact interferometer with the base up to 16 km consisting of 66 high-precision

antennas, of which 54 are 12 meters in diameter and 12 are 7 meters in diameter. The ALMA observatory is located at an altitude of 5000 m above sea level in the Atakama Desert in Chile and is capable of conducting astronomical observations in all transparency windows from 10 mm to 0.3 mm. The fully operational ALMA observatory will provide an unprecedented high sensitivity up to 50 μJy in the continuum with an angular resolution less than 0.1 arcsec, which allows detailed mapping of protoplanetary discs and studies of the morphology of distant galaxies. A small field of view is a shortcoming of ALMA, which requires long observations for carrying out large surveys of point-like sources, studying extended star formation regions in the Galaxy, and mapping large areas of the sky.

As noted above, ground-based astronomical observations at wavelengths $\lambda \lesssim 300$ μm are problematic because they are significantly limited by the properties of Earth's atmosphere: its proper thermal emission and absorption by vapors of water, oxygen, carbon dioxide, and ozone. Therefore, observations at wavelengths shorter than 300 μm have to be carried out at altitudes of 10–30 km at least, where the partial water vapor pressure strongly decreases and the associated absorption almost vanishes. This property has already been exploited by telescopes aboard aircraft (SOFIA (Stratospheric Observatory for Infrared Astronomy) [3]) or stratospheric balloons (BOOMERANG (Balloon Observations Of Millimeter Extragalactic Radiation and Geophysics) [4], TELIS (TEraHertz and submillimeter Limb Sounder) [5], Olimpo, etc.). A space telescope has clear advantages because it is free from negative effects from Earth's atmosphere and can be cooled to low temperatures, which strongly increases its sensitivity.

The Herschel Space Observatory, launched in 2009 and operated until the middle of 2013, is the most perfect and closest predecessor of Millimetron. The Herschel Observatory (http://sci.esa.int/herschel/ [6]) consists of a telescope 3.5 m in diameter with passive cooling to about 70 K. The observatory carried out observations in the wavelength range 55–672 μm. Receivers of the Herschel Observatory included CCD photometers, a CCD spectrometer with moderate resolution, and a high-resolution heterodyne spectrometer. The main scientific achievements of the Herschel Observatory include observations of star-formation and dust regions in our Galaxy and external galaxies and studies of submillimeter galaxies and Solar System bodies.

Millimetron is a new step in the development of space observatories due to unique capabilities: high angular resolution and unprecedentedly high sensitivity in a broad wavelength range from the far infrared to the millimeter. This leap forward may solve many fundamental issues of astrophysics and cosmology. The unique scientific breakthrough plans are crucial in determining the technical requirements for the Millimetron observatory.

Millimetron will be launched into orbit in the vicinity of the Lagrangian point L2 at a distance of 1.5 million km from Earth behind the Moon's orbit, with the most favorable external conditions for telescope cooling. To provide an unprecedentedly high sensitivity, deep cooling of the telescope mirrors to temperatures as low as 10 K is required. This can be realized only by joint operation of two cooling systems, passive and active. The first is based on sun shields and the second uses close-cycle cryogenic refrigerators. Being in the vicinity of the Lagrangian L2 point, Millimetron, along with a ground-based telescope or a system of telescopes, will form an interferometer with the maximum projection of the base on the plane perpendicular to the line of sight of a studied source greater than 1.5 mln km. Such a unique instrument opens new horizons in solving astrophysical problems by enabling measurements with record high angular resolution.

The Spectrum-M project started in the 1990s. A description of different concepts of the Millimetron observatory since the beginning of the project and a list of its main scientific tasks can be found in [2, 7, 8]. The main requirements for Millimetron are listed in Table 1.

Table 1. Main requirements for the Millimetron observatory.

<table>
<tr><th>Mode</th><th>Single-dish</th><th>Very long baseline interferometer (ground–space)</th></tr>
<tr><td>Possibilities</td><td>Low spectral resolution (photometry), $R=\lambda/\Delta\lambda\sim 3$
Medium spectral resolution, $R\sim 10^3$
High spectral resolution, $R\geqslant 10^6$
Polarimetry</td><td>Source angular size estimate
One-dimensional source cross section
Model mapping using a priori source structure model</td></tr>
<tr><td>Working wavelength range</td><td>20 μm – 3 mm for $R\sim 3$ and $R\sim 10^3$, 60 μm – 1 mm for $R\geqslant 10^6$</td><td>0.3 – 17 mm</td></tr>
<tr><td>Angular resolution</td><td>6 arcsec at $\lambda = 300$ μm</td><td>For a 1.5 mln km base:
~ 2 μas at $\lambda = 13.5$ mm
~ 50 nas at $\lambda = 0.345$ mm</td></tr>
<tr><td>Sensitivity</td><td>RMS noise amplitude σ
(at wavelength $\lambda = 300$ μm, exposure time 3600 s, effective telescope area 50 m^2, NEP detector sensitivity $\leqslant 10^{-19}$ W Hz$^{-1/2}$):
20 nJy at $R\sim 3$
4 μJy (or 4×10^{-23} W m^{-2}) at $R\sim 10^3$</td><td>σ for the 4 GHz band (two polarizations, two-bit quantizing)
<table>
<tr><th>Frequency, GHz</th><th>Coherent sampling time [9], s</th><th>Sensitivity, mJy</th></tr>
<tr><td>22</td><td>500</td><td>0.2</td></tr>
<tr><td>43</td><td>500</td><td>0.3</td></tr>
<tr><td>100</td><td>500</td><td>0.5</td></tr>
<tr><td>240</td><td>70</td><td>2.0</td></tr>
<tr><td>640</td><td>10</td><td>20.0</td></tr>
<tr><td>870</td><td>5</td><td>40.0</td></tr>
</table></td></tr>
<tr><td colspan="3">* NEP — Noise-equivalent power.</td></tr>
</table>

Table 2. Expected parameters of Millimetron in the single-dish mode and main capabilities of other observatories and telescopes.

	Herschel	ALMA	SPICA	Millimetron
Range, μm	50 – 670	315 – 9680	5 – 210	20 – 3000
Resolution, arcsec	3.5 – 40	0.01 – 5	0.3 – 14	5 – 60
Field of view	up to $4' \times 8'$	up to $25''$	$5' \times 5'$	$6' \times 6'$
Sensitivity* σ, sampling time 3600 s				
Photometry	1 mJy	> 10 μJy	4 μJy	20 nJy
Spectroscopy ($R \sim 1000$)	20 mJy	60 μJy	200 μJy	4 μJy
Spectroscopy ($R \geqslant 10^6$)	2 Jy	50 μJy		200 mJy

* Sensitivity depends on the working wavelength, which are shown here for $\lambda \sim 200 - 300$ μm.

We note that Table 1 presents desirable requirements that can be realized at the present technology readiness level. The final requirements to the observatory will be formulated based on a careful compromise among the desirable capabilities, the priority of the scientific tasks, and the project cost.

A comparison of the expected capabilities of the Millimetron Observatory with those of the existing and planned instruments for observations in nearby or similar wavelength ranges (Table 2), such as the ground-based ALMA observatory and the Herschel and SPICA (Space Infrared Telescope for Cosmology and Astrophysics) [10] space telescopes, allows compiling a list of the highest-priority scientific tasks and formulating the priority of observations.

The expected sensitivity of Millimetron, as a minimum, is two orders of magnitude higher than that of the Herschel telescope. The present-day record angular resolution in the 20–300 μm range is much worse than in other ranges (radio and near-IR). This is because the 20–300 μm range is virtually inaccessible for ground-based observations, and all space telescopes launched so far have had small apertures $\lesssim 1$ m. Presently, the Herschel Space Telescope has the largest mirror (3.5 m in diameter) optimized for observations in the FIR range. For deeper studies of different astronomical objects, a better angular resolution is needed, and the Millimetron Observatory is planned to be the next step by increasing the angular resolution in the FIR range up to three times.

The angular resolution of the telescope is also related to the well-known astronomical problem, confusion: at a low angular resolution, distant sources merge into a homogeneous background, which hampers the measurement of individual fainter objects. In the FIR range, this background is usually called the Cosmic Infrared Background (CIB). The CIB is thought to be mainly due to emission from distant galaxies. Preliminary estimates show that Millimetron, with its 10 m main mirror aperture, will be capable of resolving more than 90% of the CIB into individual sources — remote galaxies (Fig. 1b).

At wavelengths longer than 300 μm, ALMA has a better angular resolution than Millimetron, and the ALMA sensitivity at longer wavelengths ($\lambda > 1$ mm) is also higher than that of Millimetron due to the huge collective area of all antennas. However, at wavelengths shorter than 300 μm, which are inaccessible to ALMA, Millimetron will have no competitors in sensitivity. A wide field of view of Millimetron is another advantage. This field of view is provided by several thousand detectors and enables Millimetron to map large areas of the sky. A grating spectrometer will offer broadband spectral measurements, facilitating measurement of redshifts of distant galaxies, which is a difficult task for ALMA.

Clearly, some observation tasks for ALMA and Millimetron can and should complement each other. In addition, another ambitious project, the James Webb Space Telescope (JWST) (http://www.jwst.nasa.gov), operating at shorter wavelengths, can be an interesting complement. For example, in studies of high-redshift galaxies, Millimetron can analyze a relatively cold molecular and atomic gas, JWST can study properties of a hot atomic gas, and ALMA can provide detailed imaging of these galaxies.

In the interferometer mode, the Millimetron Observatory can complement the Event Horizon Telescope (EHT) [11] (http://www.eventhorizontelescope.org), which is currently under development and in the near future will unify all the largest ground-based submillimeter telescopes and observatories.

This paper is prepared as a result of discussions of the scientific tasks of Millimetron at seminars and several symposia.[1]

The sections of the paper correspond to different astrophysical topics to which Millimetron can significantly contribute. The interferometric mode of observations is assumed to be used in tasks formulated in Sections 2.4, 4.2, 4.5, 5.1–5.5, 7.2; to solve tasks described in other sections of this paper, the single-dish mode of observations can be used. We note that the list of scientific tasks presented here is preliminary, and we expect the broad scientific community to produce both new and unique scientific tasks and more detailed elaboration of the proposed ones. In June 2014, the principal scientific tasks of the Millimetron Observatory were discussed at an international symposium in Paris.[2] Using the results of this symposium and based on the preliminary list of scientific problems presented in this paper, the scientific program of the Millimetron Observatory will be prepared, which will include the highest-priority tasks and a plan for carrying them out.

2. Interstellar medium and star formation regions in the Galaxy

2.1 Structure and kinematics of the interstellar medium

Currently, the problem of star formation [12], as well as its relation to the general evolution of the interstellar medium (ISM), is an important astrophysical issue. Observational data suggest that the birthrate of new stellar and planetary systems and their parameters are determined by the basic properties of the ISM: its structure, kinematics, pressure, temperature, magnetic field, and matter returned to the ISM from evolved stars. The environmental effects in the Galaxy (accretion and ram pressure of intergalactic matter, interaction with other galaxies) can also play an important role.

The global scale of the star formation process means that it is to be investigated in the general context of structure,

[1] See the report by V N Lukash and I D Novikov at Groningen (2013) http://www.sron.rug.nl/millimetron/MillimetronWorkshopGroningen2013?action=AttachFile&do=get&target=Millimetron_Workshop_SRON_2013_2_3.pdf, https://streaming1.service.rug.nl/p2gplayer/player.aspx?path=cit_mobiel/2013/04/12/3/video_post.wmv&mediatype=recordings.

[2] http://workshop.asc.rssi.ru/.

kinematics, and evolution of the ISM using as broad a sample of objects as possible. The densest ISM regions in which star formation occurs have a low temperature and therefore require observations in the FIR and submillimeter ranges, which can be done only from space. For a deeper study, a high sensitivity is also necessary, resulting in the requirement of large-size telescope mirrors and cooling, as well as increased demands for the detector parameters. The Millimetron project satisfies these requirements.

The most promising targets to be observed by Millimetron include cold (10–20 K) gas and dust clumps that are difficult to detect with less sensitive instruments, 'hot cores' and high-speed bipolar outflows, diffuse clouds, submillimeter masers, and the ISM of other galaxies.

Millimetron will study the general characteristics of the interstellar medium in different galaxies, the statistical properties of dense condensations, the structure and kinematics of interstellar clouds, the earliest stages of star formation, the mechanisms of massive star formation, the structure and properties of circumstellar shells and planetary nebulae, and the synthesis and proliferation of different molecules in the ISM, including complex organic molecules.

The high sensitivity of Millimetron in the single-dish mode will allow observations of individual clouds with a characteristic temperature about 20 K and the mass of one solar mass ($M_\odot$) at the distance up to 1 Mpc. The molecular cloud complex Sgr B2, in which many molecules were found that play an important role in the cooling and condensation of clouds, including the molecular ion H_3O^+, can provide an example. This ion, which is a result of dissociative recombination, decays into water or hydroxyl, and is very important for the overall understanding of the chemistry of oxygen in the ISM.

The submillimeter radiation from molecules and atoms arises at much lower temperatures than in the visible and infrared ranges. This means that analyzing the submillimeter data allows examining the cold ISM, in particular probing the content of hidden hydrogen [14]. The most important spectral lines of these observations include HD transitions at a wavelength of 112 μm and [CII] at 158 μm. Very interesting for ISM research is the molecule HeH^+ (the transition $J = 1-0$ at a wavelength of 149 μm), which has not yet been detected in space. The conditions of the formation and excitation of this molecule are substantially different from those of the majority of interstellar molecules. Models (e.g., those in [15, 16]) indicate that HeH^+ should be especially abundant near the sources of extreme ultraviolet (UV) and X-ray radiation.

An important area of research is the study of the ISM diffuse component by the absorption lines of different molecules at submillimeter wavelengths. The Herschel space telescope has already demonstrated the great potential of such research. In particular, it allows determining the rate of ionization by cosmic rays in various regions (OH^+, H_2O^+, and H_3O^+ lines), the turbulence dissipation rate (CH^+ and SH^+ lines), and the total distribution of molecular hydrogen (HD line). Such measurements require a sufficiently bright background source. For Millimetron with its much greater collecting area, the number of such sources will be much higher than for the Herschel space telescope, which opens up the possibility of a much more complete coverage of the galactic plane.

Another source of information about the structure and kinematics of the interstellar medium is the polarization measurement, which helps to explore the structure of magnetic fields in star-forming regions.

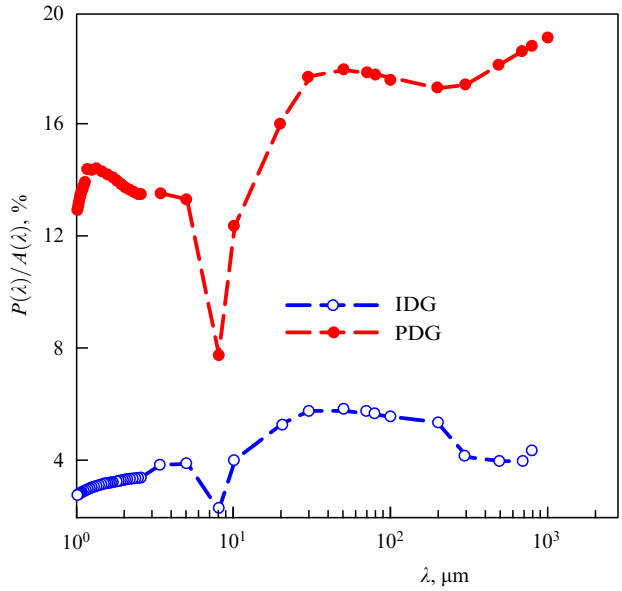

Figure 2. Polarization efficiency curve for Perfect Davies Greenstein (PDG) (the upper curve) and Imperfect Davies Greenstein (IDG) (the bottom curve) alignment of interstellar dust grains [17]; P is the polarization degree at the wavelength λ in percent, $A(\lambda)$ is the interstellar absorption at the wavelength λ.

Ground-based observations of polarization in the FIR and submillimeter ranges can be carried out only in certain transparency windows. The possibility of constructing the so-called polarization curve, i.e., the dependence of the polarization efficiency on the wavelength, would allow explaining not only the structure of the magnetic field in the star-forming regions but also the mechanism of dust particle alignment (Fig. 2).

Observations of dust emission in the submillimeter range are an important source of information about star formation. Modern data obtained by the Herschel space telescope show that star formation occurs in thin (< 0.1 pc) gas–dust filaments. The parameters of these filaments are not fully determined, and in particular the role of the magnetic field in their formation is not clarified. To answer this question, we need higher angular resolution and sensitivity (better than those of the Herschel telescope), and the possibility to measure polarization. The parameters of the Millimetron space observatory satisfy these requirements. In addition, the contribution of Millimetron to star formation and evolution studies is associated with the possibility of observing more distant star-forming regions, including extragalactic ones. In recent years, a new paradigm (in which the primary role is given to large-scale star formation complexes [18–22]) is being developed based on observational data obtained by the Herschel telescope and new theoretical research. The heuristic role of this new paradigm is extremely important, because it relates a large variety of phenomena: from spiral arm and interarm flows several kiloparsecs in size to cores of molecular clouds and protostellar condensations as small as several astronomical units (AU). However, many aspects of the star formation process remain unclear and poorly investigated. Observations of IR lines at the wavelength of 158 μm show that the galactic disc contains a large amount of CO-dark molecular gas [23]. Theoretical studies of

the formation of gas clouds in the Galaxy also show that the temperature and density of molecular clouds strongly vary (see, e.g., the phase diagram in [22]), which may indicate the existence of large masses of gas mostly consisting of molecular hydrogen with a rather low CO abundance. The distribution and parameters of this gas have been studied only in a narrow band of the galactic plane, and only in selected directions. Therefore, measurements of the relative velocities and positions of gas clouds emitting in [CII] lines at 158 μm, as well as of submillimeter and millimeter radiation of dust, are needed to determine the development mechanisms of star formation complexes, because such measurements are the basis of studies of the morphology, kinematics, and evolution of these large-scale objects.

The collective outflows of matter from the forming star clusters are another virtually unexplored important type of motion in star-forming regions. It is known that all star clusters eventually dispose of their parent gas. Clumps of molecular gas in the direction of forming star clusters in star-forming region S235 are likely to represent such collective outflows [24, 25]. A deeper understanding of the collective outflows from forming clusters requires observations of CO-dark molecular gas in the [CII] lines at the wavelength of 158 μm, which can be effectively carried out by Millimetron.

Studies of objects with large angular dimensions should be preferably carried out step by step. At the initial stage, it is necessary to determine the overall distribution of the radiation in a test line with a matrix spectrometer in the broadband spectroscopy mode with an average spectral resolution. To study the detailed kinematics, a high-resolution spectrometer is proposed to be used in a number of key areas identified in the first phase of the Millimetron observations or using data obtained previously by other instruments.

2.2 Star formation regions in the Galaxy

Spectroscopic observations with high resolution will allow a detailed study of the molecular structure of protostellar objects. Here, of particular importance are studies in the short-wavelength range of Millimetron at wavelengths less than 300 μm. The number of lines in this spectral range is smaller than in the longer wavelength region [26], which facilitates both the identification of lines and their analysis (Fig. 3). The number of lines is still very large, including both simple species lines and lines from complex organic molecules, which are interesting from the astrobiology standpoint. Some of the available line transitions for Millimetron observations are presented in Table 3.

The high spectral resolution ($\sim 10^6$) and high sensitivity achievable in the Millimetron project in observations of molecular lines allow characterizing the physical parameters and motion of gas in protostellar objects.

One of the most interesting lines shown in Table 3 belongs to atomic oxygen. The OI line at the wavelength of 63 μm significantly contributes to the cooling of the warm ISM and photodissociation of regions with high density and intensive UV radiation. Observations of this line are needed to study the energy balance in the ISM, but none of the existing instruments can observe this line. Observations of the 63 μm line by Millimetron will provide information about the content of oxygen in the interstellar medium and will help to solve the problem of the intensity ratio of the 63 and 145 μm oxygen lines detected in observations by the ISO (Infrared Space Observatory) [27]. Joint observations of lines of

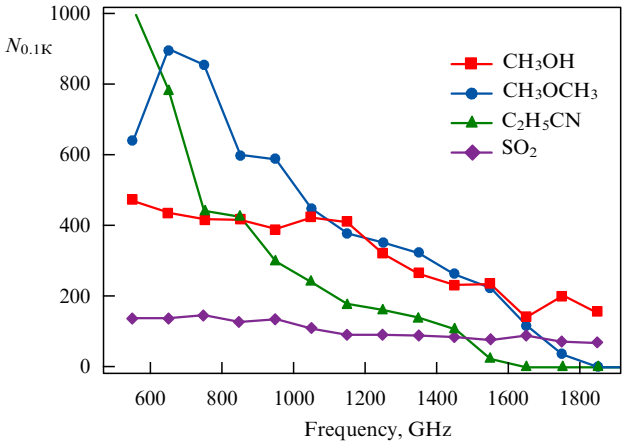

Figure 3. Predicted number $N_{0.1\,K}$ of some molecular lines with maximum emission at a temperature above 0.1 K as a function of frequency [26].

oxygen, water, molecular oxygen, and hydroxyl will help to explain the chemical evolution of oxygen compounds.

The rate of accretion onto protostellar objects is one of the key questions in protostellar evolution studies. Because direct measurements of the accretion rate are very difficult, it is usually inferred from molecular outflow parameters [28], for example, using CO observations. However, to understand the transition from the outflow rate to the accretion rate, more information is required: the velocity and size of the outflow, the inclination of the system, and the parameters of the surrounding material. Observations of the 63 μm [OI] line will measure the accretion rate in a more direct way, but this will also require high angular and spectral resolutions.

Another way of probing the accreting matter is to observe absorption lines, which would guarantee that an absorbing material is in front of a growing protostar. Recently, it was shown in [29] that a promising line in this respect could be an ammonia line at the wavelength of 166 μm. FIR spectral observations by Millimetron will provide an opportunity to study accretion onto protostars with a spatial resolution four

Table 3. Important submillimeter transitions in atoms and molecules.

Atom/molecule	Frequency, GHz
CI	492, 809
OI	2060, 4745
HD	2675, 5332
OH	1835, 2510, 3789, ...
CH	537, 1477, 1657, 2007, 2011, 4056, 4071, ...
HF	1232, 2463
H_2O	557, 988, 1113, 1670, 2774, 2969, ...
HDO	465, 894
CII	1901
NII	1461, 2459
OIII	3393, 5787
NIII	5230
HeH^+	2010, 4009
OH^+	972, 1033, 1960, ...
CH^+	835, 1669, ...
SH^+	526, 683, 893, 1050, ...
H_2O^+	1115, 1140, ...
H_3O^+	985, 1656, ...
H_3^+	3150
H_2D^+	1370, 2577
D_2H^+	1477

times that of the SOFIA telescope. This gain in spatial resolution can be critical for star-formation studies.

Observations of neutral oxygen and ionized carbon lines with high angular and spatial resolutions are valuable to probe the evolution of ionized hydrogen zones. In particular, numerical simulation shows that the extent of the ionized carbon region around a young massive star significantly depends on the parameters of the star and the surrounding gas density [30].

One of the tasks of the Millimetron operations will be high-resolution spectral surveys covering frequency bands of a few tens or hundred GHz. Millimetron's high sensitivity and lack of atmospheric absorption will enable surveying weak and hence poorly studied sources (for example, 'hot corinos' — hot regions near low-mass protostars). As a result, in addition to determining the main physical parameters and molecular composition of these sources, new molecules can be detected, including those important from the standpoint of astrobiology.

One of the tasks of the Millimetron Space Observatory will be to study cosmic masers in the millimeter and submillimeter wavelengths in the single-dish mode. Bright masers occur in the water vapor line $6_{1,6}$–$5_{2,3}$ at 22 GHz. However, there are other known H_2O maser lines in the submillimeter wavelength range. Submillimeter lines of water vapor are difficult or even impossible to observe from Earth due to strong absorption in the atmosphere, and hence observations of H_2O masers are carried out almost exclusively at the frequency of 22 GHz. As a result, not even a very rough model of these objects can be built. Some progress in observations of submillimeter maser lines have been made at high-altitude astronomical observatories and using the space-based observatories SWAS (Submillimeter Wave Astronomy Satellite), Odin, and Herschel. Further progress will be possible after the launch of Millimetron, which will be the best submillimeter maser observatory among space observatories to be launched within the next 10–15 years.

2.3 Protoplanetary discs and protostellar objects

One of the key issues in the physics of protoplanetary discs (PPDs) is their mass. Presently, to determine PPD masses, mainly millimeter dust emission observations are used, under the assumption that the dust is well mixed with the gas. However, the sensitivity of modern telescopes is insufficient for detecting low-mass and distant PPDs. There are many discs for which only the upper limits of radiation fluxes (< 10 mJy) have been established. Only an accurate disc mass evaluation can clarify whether the disc is able to start forming a planetary system. It would be highly desirable to find a direct indicator of the gas mass. Presumably, HD molecule radiation (Fig. 4) at 112 and 56 μm [31] could be such an indicator.

One of the biggest challenges for Millimetron may be observations of water in PPDs. In these objects, both 'warm' (close to the star) and 'cold' (more distant) water reservoirs are possible. At present, water is commonly viewed as being the main factor determining the structure of planetary systems (the 'snow line'). Observations of water lines by the Herschel space telescope were carried out only for a few PPDs, and observations of cold water in them yielded conflicting results [32, 33]. Obviously, to clarify the role of water in the formation of planetary systems, a more significant sample is needed, which requires instruments with greater sensitivity and better angular resolution. The

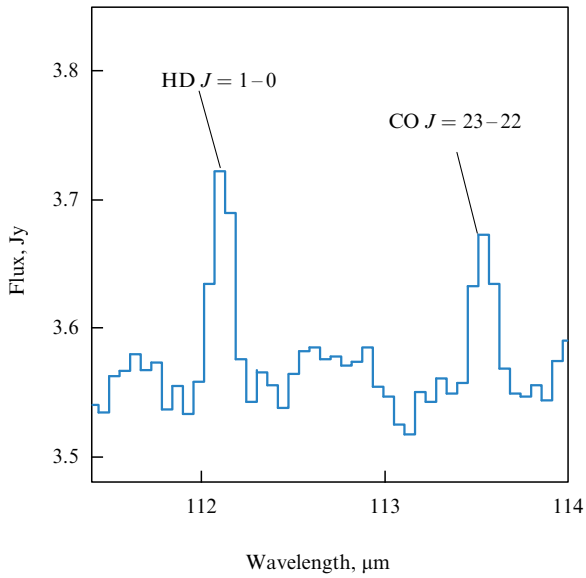

Figure 4. HD molecule line in the spectrum of a protoplanetary disc around TW Hya (http://cosmos.esa.int/web/herschel/home).

combination of water lines in various parts of the Millimetron range will allow reaching conclusions about the spatial distribution of water in the disc, in particular, about the actual location of the snow line.

Observations of the PPDs of molecular oxygen and of the vibrational–rotational lines of organic and simple compounds in regions of planetary formation, as well as of less common isomers of previously detected molecules (or those discovered by ALMA) will also be feasible. High temperatures (over 100 K) in planetary formation regions at the distances less than 5–20 AU from the star result in populating high transitions, especially in complex molecules. An example is provided by the detection of organic molecules in the inner parts of the discs with the Spitzer telescope (see, e.g., [34]). Calculations of the PPD chemical structure in [35] show that the column densities of molecules such as methyl cyanide and formic acid, with lines in the Millimetron range, reach large values in planetary formation regions.

In the submillimeter (100 μm) range, observations of large particles forming in PPDs are possible. It is very important to properly calibrate receivers with a wide and continuous spectral coverage. Figure 5a shows the theoretical spectra of a PPD in the globule CB26 in comparison with Herschel telescope observations. Error bars indicate the flux calibration uncertainty. The figure shows that in order to find the mass distribution and size of dust particles, high-precision observations of discs at wavelengths of about 100 μm are needed. To solve this problem, the single-dish mode is sufficient.

FIR spectroscopy with a moderate spectral resolution allows detecting bright CO and water and determining the parameters of the PPD inner regions.

In addition to the PPD studies, searching for and studying cold gas and dust clouds in the Galaxy is an important task. One of the main sources of information about the physical conditions in prestellar and protostellar objects is their broadband spectral energy distribution (SED). It is SED that became the basis for the currently accepted classification of these objects. Moreover, for objects of class −1 (prestellar

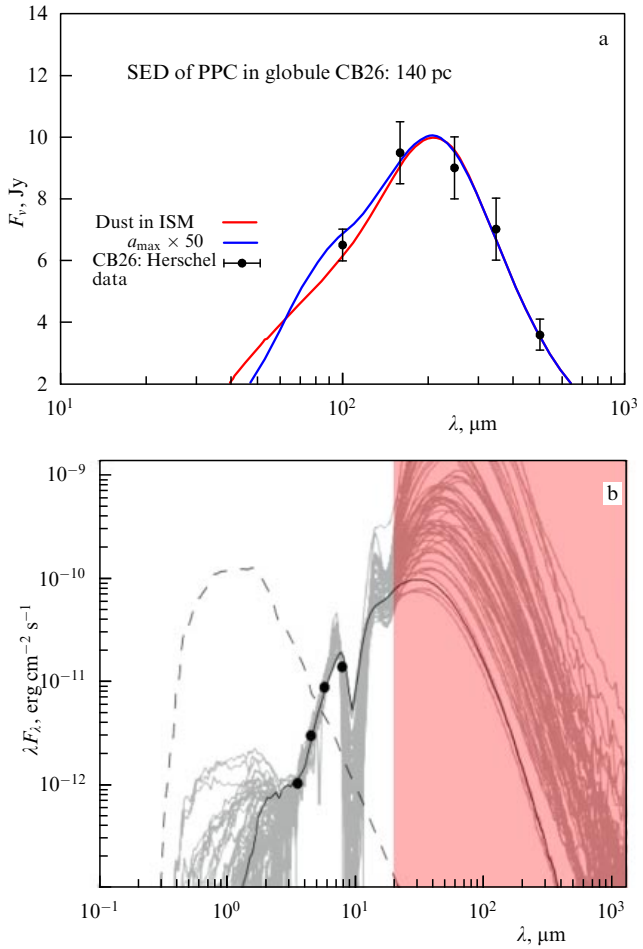

Figure 5. (In color online.) (a) Spectral energy distribution (SED) of the protoplanetary disc in globule CB26 observed by the Herschel telescope. The red curve is a model of the dust with typical ISM parameters (the maximum grain size $a_{max} = 0.25$ μm), the blue curve is a model for a_{max} 50 times larger than the typical value (calculations according to the model in [36]). (b) Fitting of the observed near-IR spectrum (black dots) from a typical protostellar object. The formal best-fit solution is shown by the thick black curve. The grey curves show spectra of objects with masses from $M_\odot$ to 10 $M_\odot$, which equally well fit the observed near-IR data but significantly deviate in the FIR (http://caravan.astro.wisc.edu/protostars/). The dashed curve shows the best-fit solution for the photosphere emission from the central source.

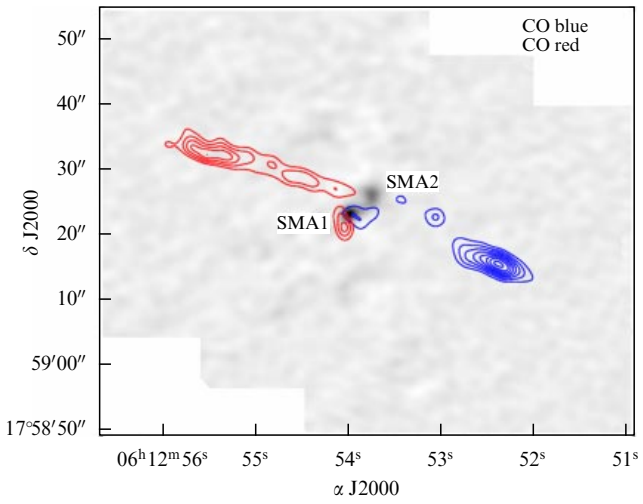

Figure 6. (In color online.) Example of a high-velocity bipolar outflow. Blue and red contours respectively show the emission in the blue and red wing of the CO(3–2) lin. Sky coordinates α, δ (epoch J2000) [41].

core) and 0 (the earliest stage of evolution in the presence of a central IR source), the spectral maximum falls in the FIR and submillimeter range. A space telescope will allow building SEDs of prestellar cores without breaks caused by atmospheric transparency windows. The detailed spectral profile will clarify the evolutionary status of a specific core. Until now, the identification of a core as being pre- or protostellar has been based on the absence or presence of a compact source in the core. The relative number of prestellar and protostellar objects forms the basis for estimating the relative duration of the corresponding evolutionary stages. However, for example, observations of the low-mass core L1014 by the Spitzer space infrared telescope revealed the presence of a weak compact internal source by excess radiation at wavelengths less than 70 μm [37].

In [38], the existence of such a problem was also shown for massive cores. Observations of two massive cores of infrared dark clouds (IRDCs) were analyzed in [37]. Near-IR and millimeter studies classified these cores as starless. But the analysis of the spectrum at the wavelength of 70 μm revealed that in both cases the cores already conceal compact sources of radiation — protostars.

The reasons for the importance of the 50–150 μm range are illustrated in Fig. 5b, which shows the result of fitting the near-IR spectrum of a typical protostellar object with a model presented in [39, 40]. The best fit is formally shown by the solid black curve. However, similar fits can be obtained by other models with the object mass ranging from $M_\odot$ to 10 $M_\odot$. Figure 5 clearly shows that the maximum emission of a typical protostellar object falls in the FIR range. Including the data on the radiation at 70 μm into the model of the same object reduces the mass calculation uncertainty threefold.

The 50–150 μm range was available for observation by the Herschel space telescope. However, the lack of high angular resolution of the instrument did not allow a detailed investigation of protostellar objects at long distances, which significantly restricts their sample. The higher angular resolution of Millimetron enables observations at longer wavelengths. In particular, using the PACS (Photodetector Array Camera and Spectrometer) detector of the Herschel telescope (70, 100, and 160 μm), many point-like objects inside many IRDCs were discovered [42]. However, such point-like objects were not resolved at longer wavelengths (250–350 μm). The temperature, mass, and luminosity of these sources need to be determined more accurately. The high sensitivity of Millimetron will help to discover more compact protostellar sources by including distant and (or) denser objects in the statistics.

In addition to the cold gas and dust clouds in star-forming regions, hotter objects have been detected. They show a dust continuum and numerous spectral lines of gas-phase molecules. The spectral energy distribution in such objects is still poorly explored, but is a very important task.

Another important field of research is the study of high-velocity bipolar outflows formed by accretion discs around protostars and young stars (for example, the object S255IR that emits in the 1.1 mm continuum) (Fig. 6). By external appearances, a bipolar outflow is similar to a black hole jet, which suggests the possible similarity in physical mechanisms

of both phenomena. The origin of bipolar outflows is still uncertain, and their study is therefore relevant.

As a related problem, we also mention the submillimeter observations of asteroids and comets. Observations of asteroids in the reflection (scattering) light cannot deliver reliable information about their size, because their albedo has to be assumed. Observations of the proper radiation of asteroids are more reliable in this respect. In addition, the emission spectra of asteroids allow not only evaluating their size but also obtaining information on the chemical composition and surface structure [43]. However, the temperature of asteroids (especially far from the Sun) is low, and hence their emissions fall in the infrared and submillimeter range, which requires space observations. Spectral observations of comets make it possible to clarify their molecular composition and obtain information about the evolution of matter in the early Solar System.

2.4 Maser sources

Maser quantum transitions in molecules are a powerful tool for studying various astrophysical sources, such as accretion discs around supermassive black holes in galactic cores, protostellar/protoplanetary discs and outflows from young stars in star-forming regions, interaction regions of expanding HII regions and supernova remnants with dense surrounding gas clumps, and expanding shells and jets associated with evolved stars [44, 45]. Observations of masers are widely used to detect sources with unique physical and evolutionary status, to measure their distances, and to study their parameters, their kinematics, and the structure of accretion discs [46-48]. The modern scientific projects Radioastron, BeSSeL (Bar and Spiral Structure Legacy Survey), MCP (Megamaser Cosmology Project), and MMB (Methanol Multibeam Survey) demonstrate the great potential for maser observations as a research tool. The value of this instrument is determined by precise measurement of the positions of the objects. Because maser sources have a small angular size, observations in the interferometry mode are the most important.

In the ground–space VLBI (GSVLBI) mode, the receiving equipment of Millimetron allows observations of water masers at the transition frequency 22235.08 MHz. The possibility of maser observations in the GSVLBI mode was shown by the Radioastron space mission.

The scientific program to study cosmic masers using the ground–space interferometer Radioastron included observations of 19 water molecule maser sources. These masers are very compact objects (often not even resolved using the largest ground-based bases) that have the highest brightness temperature, sometimes exceeding 10^{17} K [49]. Because of these properties, masers can be used for high-precision studies of the kinematics and physical parameters of objects in our and other galaxies. Observations by ground–space interferometers have allowed resolving the most compact components and evaluating the brightness temperature of the maser source and its size, which is necessary to clarify the pump mechanism and to model the emitting region. During studies, the water line radiation at 22 GHz from extremely compact maser components in the directions to the four star-formation regions was detected: Orion A, W31RS5, W51M/S, and Cepheus A [50].

Some sources (Cepheus A) show the presence of very compact substructure maser details with a size of the order of 10 micro-arcseconds (which corresponds to 0.007 a.u.). Moreover, the objects move with a high relative velocity. This means that the maser source has a complex spatial and kinematic hyperfine structure on scales comparable to the size of the Sun. This picture is probably an indication that in this case, the maser emission arises from protostellar/protoplanetary discs or the smallest turbulence cells corresponding to the dissipation scale. For discs of all types, the most important and still unsolved problem is the angular momentum transfer mechanism [51]. Turbulent viscosity is classically considered to be such a mechanism, but there is still no consensus on the turbulence onset mechanism [51, 52].

The Millimetron equipment allows observations of masers in the submillimeter range, as well as of masers formed in other galaxies and in evolved stars, which requires a sensitivity better than that of Radioastron. At the moment, the possibility of observing in the GSVLBI mode is confirmed only for masers in star-forming regions of the Galaxy at hydroxyl and water molecule centimeter transitions.

3. Stars and planets

3.1. Direct observations of exoplanets

One of the promising methods for studying extrasolar planets is their direct observation.

In the single-dish mode, Millimetron is able to observe massive planets far from the central star. The more distant the system is, the larger the orbital radius of the planet should be in order to be resolved by a telescope. Unfortunately, Earth-like planets at such distances have a very low radiation intensity, and therefore only gas giants are observable in this mode. Table 4 lists extrasolar planets (as of the end of 2013) that will be available for direct Millimetron observation. Only three planets from this list could be observed by the Herschel telescope, and in addition the planet Fomalhaut b was observed at the sensitivity limit. Two planets shown in Table 4 were discovered after the Herschel telescope operation had been completed. We note that in the range of Millimetron measurements, the star and a remote gas giant have the lowest contrast, which facilitates their observation [53].

Observations of known transiting planets are of particular interest. Observations of planetary transits and antitransits allow determining the orbital parameters of the planet and its mass and radius and obtaining the absorption spectra of the upper layers of its atmosphere. Since 2003, there has been a series of detailed spectroscopic observations of transits and antitransits of different types of exoplanets [54–58]. The high accuracy of Millimetron enables spectroscopic observations of transits and antitransits and thus allows obtaining unprecedentedly comprehensive information about these systems.

3.2 Mass loss at late stages of stellar evolution

At the late evolutionary stages, low- and intermediate mass stars (which include the Sun) experience an intensive mass loss. This is expressed in an expansion of the stellar envelope with the subsequent transformation into a planetary nebula. Studies of the circumstellar medium during and after the asymptotic giant branch (AGB) are also closely related to the ISM enrichment by heavy elements.

The high capabilities of space research of low- and intermediate-mass stars in the infrared range were demonstrated by key programs of the Herschel telescope such as

Table 4. Exoplanets available for Millimetron observations.

Name	Mass* M/M_J	Semi-major axis, a.u.	Distance, pc	Stellar type	Age, bln yrs	Effective temperature, K	Herschel
Fomalhaut b	3	115	7.704	A3 V	0.44	8590	Limit
HN Peg b	16	795	18.4	G0 V	0.2		yes
WD 0806-661B	8	2500	19.2	DQ D	1.5		yes
AB Pic b	13.5	275	47.3	K2 V	0.03	4875	no
Ross 458 (AB)	8.5	1168	114	M2 V	0.475		no
SR 12 AB c	13	1083	125	K4-M2	0.001		no
FU Tau b	15	800	140	M7.25	0.001	2838	no
U Sco CTIO 108	16	670	145	M7	0.011	2600	no
HIP 78530 b	23	710	156.7	B9 V	0.011	10,500	no
GU Psc b	11	2000	48	M3	0.1	—	—
HD 106906b	11	654	92	F5V	0.013	6516	—

* M is the exoplanet mass, M_J is the mass of Jupiter.

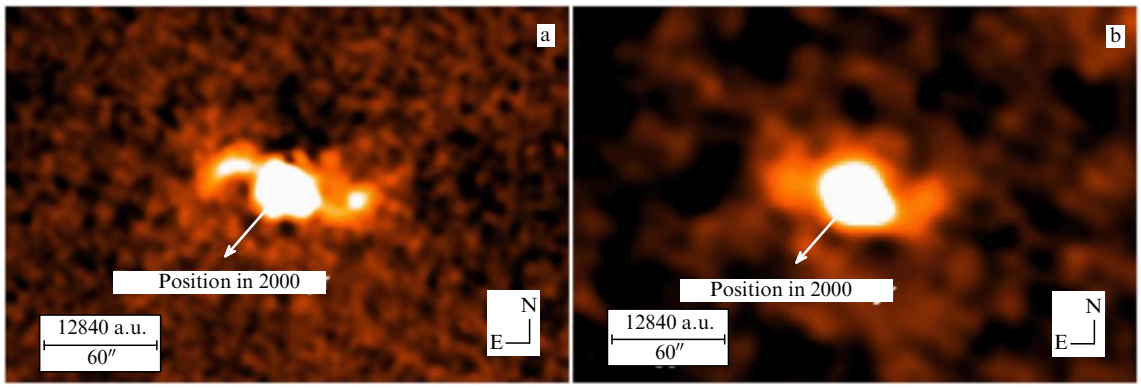

Figure 7. (In color online.) Image of the star R Aqr in the continuum at wavelengths (a) 70 μm and (b) 160 μm. Arrows show the proper motion of the object [59].

HIFISTARS, "the circumstellar environment in post-main-sequence objects," and others.[3] Higher angular resolution, sensitivity, and the wide range of Millimetron will not only significantly improve the quality of research of evolved stars but also define a number of new challenging tasks in the study of these objects.

Observations from the high-resolution spectrometer, in particular, will allow the following studies.

• *Kinematics of outflows from AGB stars.* Millimetron allows observations of the most highly excited molecular lines of CO and H_2O, and other lines formed close to a star. Such observations are impossible with other instruments, including the Herschel telescope, and will help to answer a number of important issues related to the outflow mechanism. For example, according to modern concepts, the radiation pressure on the dust in oxygen stars is not large enough to explain the observed mass loss rates.

• *The cause of the asymmetry of stellar shells, symmetric at the AGB stage and asymmetric at the stage of protoplanetary and planetary nebulae.* Currently, there are several hypotheses. One of them is related to the binarity of the star [59]. To confirm or refute this hypothesis, observations with high angular resolution are required, which are possible with Millimetron.

• *The composition and physical parameters of the interaction regions of shells of moving evolved stars with the environment.* Observations by the Herschel telescope revealed the presence of complex structures and motions in such objects, which allows investigating the stellar envelope, circumstellar medium, and motion of the stars [59, 60] (see Fig. 7).

• *The formation of molecules and dust in the shells of evolved stars* [61, 62].

The use of a short-wavelength matrix spectrometer, in particular, will allow carrying out the following studies:

— observations of extended planetary nebulae in the [NIII], [OIII], [OII], [CII] lines, etc., to study the dependence of the chemical composition and physical parameters of the gas on the distance to the star. The method that was developed in [63] will be further improved to analyze the Millimetron data with better sensitivity. These studies are related, in particular, to the problem of the origin of hydrogen-poor stars:

[3] http://Herschel.cf.ac.uk/key-programmes/stars.

— observations of clumps and other irregularities in the structure of extended planetary nebulae to study temperature and density variations, which largely determine the chemical composition and evolution of these objects;

— studies of the structure of stellar shells interacting with the environment. These studies also require observations using matrix instruments.

3.3 Search for extraterrestrial life

Due to the absence of an atmosphere, the Millimetron observatory will be capable of studying many spectral lines of water molecules and more complex organic compounds that are difficult or impossible to observe from Earth's surface. The study of these lines in the Solar System and PPDs would help to determine the origin and primary molecular composition of Earth's oceans and to draw conclusions about the abundance of planets containing liquid water on the surface, and therefore having suitable conditions for life.

For years, the search for manifestations of extraterrestrial civilizations has been one of humanity's most ambitious projects. Major efforts are now focused on the interception of messages from extraterrestrial civilizations, and the millimeter range is promising for these purposes. The advantages of this range for directed transmission in the midsection of the cosmic microwave background were discussed in [64]. A characteristic marker of this region of the spectrum can be the positronium hyperfine splitting line at 203 GHz ($\lambda = 1.5$ mm), an analogue of the 21 cm line of the hydrogen atom. Preliminary observations have already begun [65]. The search for positronium using Millimetron is an independent important task.

Along with the search for signals from extraterrestrial intelligence, traces of astro-engineering activities are being searched for. In particular, a well-developed civilization would be able to surround a star by a system of structures intercepting and using a significant portion of the star energy (the so-called Dyson sphere [66]), which should re-emit all or part of the energy at frequencies lower than the radiation frequency of the star itself. For the Sun and a Dyson sphere with a radius of 1 AU, the temperature of the sphere would be about 300 K. It can be expected that the use of more advanced technologies would be associated with the use of lower temperatures, and the position of the emission maximum would shift from 20 μm towards longer wavelengths. Therefore, such objects would most effectively be sought in the infrared range up to the wavelength corresponding to the maximum of space radiation (1.5 mm). The first sky FIR survey aimed at the detection and spectral measurements of astronomical objects was carried out with IRAS (InfraRed Astronomical Satellite). Two hundred fifty thousand point-like sources were found. Results of the search for objects similar to the Dyson sphere are reported in [67, 68] (Fig. 8); several objects whose natural origin has still not been reliably proven were found.

Spectral parameters and their comparison with the black-body spectrum are important criteria. The spectral maximum determines the temperature. The spectral index in the long-wavelength part of a power-law spectrum is -2 for a black body and -3 and -4 for respective amorphous and metal dust particles whose size is much smaller than the wavelength. The temperature, flux, and shape of the red part of the spectrum and the distance from the source can be used to estimate the size of the source and to distinguish it from

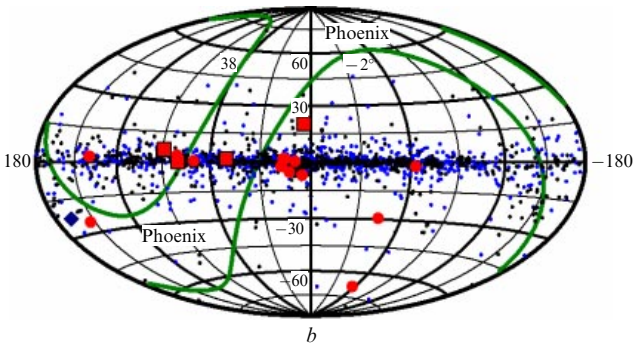

Figure 8. (In color online.) Sky location of 16 possible Dyson sphere candidates (red symbols). Three of them (red squares) show the least deviation from the black-body spectrum. The blue symbols show 2240 candidates selected from the IRAS catalogue. The green curves delineate the sky region accessible for the Arecibo radio telescope participating in the CETI program [68].

natural clouds of dust or stones emitting in the infrared range (protostellar objects, old stars). To develop a reliable criterion to search for Dyson spheres, it is necessary to investigate the properties of natural sources in detail, which can be accomplished by Millimetron.

4. Supernovae and supernova remnants

4.1 White dwarfs

FIR photometric observations of nearby cold white dwarfs allow determining their atmospheric composition, which can be used to precisely determine the age of the objects and the Galaxy.

White dwarfs are apparently the most numerous sky objects. They can be separated into two large groups: hot and cold. A cold white dwarf is an observable final stage of the white dwarf evolution; therefore, the age estimate of cold white dwarfs can be used to determine the age of the galactic disc and halo, as well as of nearby globular clusters. White dwarf cooling, which plays a crucial role in the white dwarf evolution, is not yet fully understood; it depends on the white dwarf atmosphere composition. Therefore, to determine the temperature, luminosity, and age of cold white dwarfs, their atmospheric composition should be known.

An analysis of mid-IR observations of nearby cold white dwarfs with an effective temperature less than 6000 K revealed that the maximum of emission in this range is somewhat lower than predicted by models that well reproduced the observed luminosity function at wavelengths shorter than 1 μm [69]. This situation is presented in Fig. 9, where the observed spectral energy distribution in the wavelength range from 0.1 to 100 μm is shown for cold white dwarf LHS 1126, together with model atmospheres of different chemical compositions. Clearly, to solve the problem of the atmospheric composition of cold white dwarfs, high-precision FIR measurements are required.

The expected Rayleigh–Jeans fluxes from white dwarfs at distances closer than 100 pc are about a few mJy.

An interesting problem is to search for debris cold dust discs around white dwarfs, which can be formed due to comet and asteroid collisions, by performing single-dish FIR observations. For example, white dwarf G2938 shows an FIR excess. In addition, in the atmosphere of this object, as

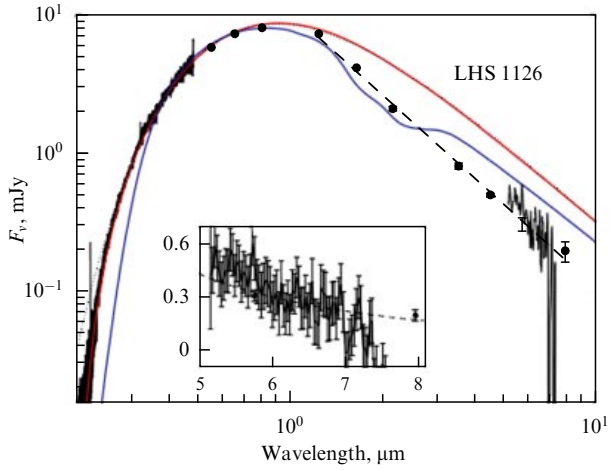

Figure 9. (In color online.) Spectral energy distribution of the cold white dwarf LHS 1125 (model) [69]. The red and blue curves show models with different hydrogen-to-helium ratios in the atmosphere. Circles with error bars show the results of observations. The dashed curve, which best fits the observations, corresponds to the spectral slope −1.99. The inset zooms the spectrum at 5–8 μm .

well as in other hot white dwarfs, heavy elements have been discovered, such as calcium and iron, which should have plunged deeper into the star due to strong surface gravity [70]. The presence of a debris cold dust disc irradiated by the emission of the white dwarf could be an explanation. More than 20 white dwarfs surrounded by dust discs are currently known from FIR observations. Presently, studies of white dwarf atmospheres 'polluted' by heavy elements are being carried out in the mid-IR range: for example, photometric data was obtained by WISE (Wide-Field Infrared Survey Explorer) [71]. Several white dwarfs demonstrate an excess in this range [72].

Recently, the presence of exoplanets around white dwarfs has been discussed. In principle, white dwarfs are sufficiently bright objects to sustain water in a liquid state on the surface of such planets. The first planet was discovered around star GI86, which belongs to a binary system with a white dwarf. Both photometric and spectroscopic studies of white dwarf atmospheres with heavy elements and of white dwarfs surrounded by dust discs, with the aim to explore the properties of the dust, examine the atmospheric composition, and discover the exoplanetary systems around them, are important and interesting tasks.

4.2 Pulsar radio emission

The spectra of most radio pulsars rapidly decrease with frequency [73]. However, some objects are observed in the gigahertz range [74–76]. Here, several new and interesting tasks can be envisaged.

Four radio pulsars (B 0329 + 54, 0355 + 54, 1929 + 10, and 2021 + 51) and two anomalous X-ray pulsars (AXP) (XTE J 1810-197 and 1E1547-5408) exhibit spectral flattening at several tens of GHz (Fig. 10a, b) or even an intensity increase when the frequency increases to 87 GHz [75]. In radio pulsars and AXPs, the 43 GHz flux density lies in the respective ranges 0.15–0.50 mJy [77] and 1–5 mJy [78, 79]. The sensitivity of the bolometer for broadband ($\gtrsim 10$ GHz) observations in the 50–200 GHz frequency range with an exposure of several dozen minutes is estimated to be around 0.1–0.5 mJy, which likely makes it possible to detect such pulsars.

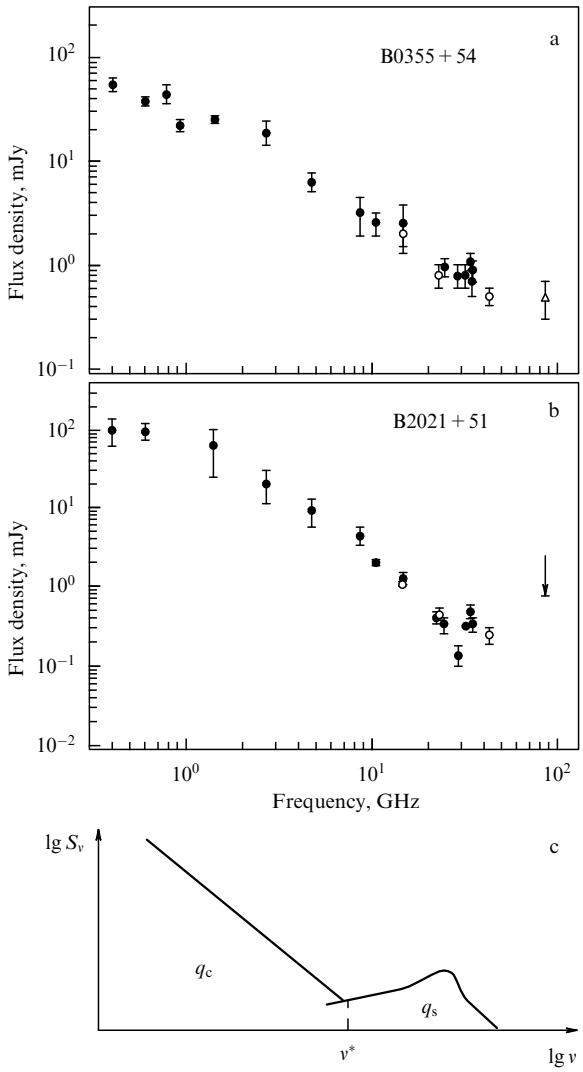

Figure 10. Spectra of pulsars B0355 + 54 (a) and B2021 + 51 (b). Measurements at 87 MHz for B0355 + 54 and B2021 + 51 are shown by the light triangle and the arrow (the upper limit), respectively. (c) Theoretical spectrum of a radio pulsar: S_ν is the flux density, q_c is the power emission generated due to cyclotron instability, and q_s is the power of synchrotron radiation.

Moreover, estimates show that the magnetic field and spin rotation axis misalignment can be small in these objects (less than 30°). In this case, the magnetosphere can extend far beyond the light cylinder, forming appreciable pitch angles of relativistic electrons (more than 0.01), and synchrotron radiation is generated [80, 81]. For typical parameters of these pulsars, the radiation intensity must increase with frequency starting from a few tens of GHz. For the usually assumed pulsar parameters, the maximum frequency is $\nu_{max} \sim 3 \times 10^{11}$ Hz. Qualitative estimates of the millimeter intensity increase are model-dependent. For a monoenergetic relativistic energy distribution, the intensity increases as $\nu^{1/3}$, suggesting a twofold intensity increase at 275 GHz compared with 34 GHz. For a power-law electron energy distribution and assuming a large optical depth of the emitting region, the intensity increases as $\nu^{2.5}$, and the intensity increase at 275 GHz can be as high as 200 times (Fig. 10c). Testing these predictions is important for deeper insights into the models of magnetospheres of both radio pulsars and AXPs.

Polarization measurements of pulsars with an increased flux density at several tens of GHz play an important role. The degree of polarization of ordinary pulsars typically decreases with frequency. Switching on the synchrotron mechanism should increase the degree of polarization. The confirmation of this property would be an additional argument supporting the synchrotron radiation hypothesis for pulsars. In addition, the pulse profile generated by the synchrotron mechanism is different from profiles expected in other models. Therefore, the pulse profiles in the millimeter range can be different from those at lower frequencies.

In parallel with spectral observations, it is necessary to measure the angular size of the emitting region in pulsars. Nonthermal pulsar radio emission is assumed to be generated inside the light cylinder with the radius

$$r_{\rm LC}\ [\rm cm] = \frac{cP}{2\pi} = 4.8 \times 10^9 P\ [\rm s]\,,$$

where P is the pulsar spin period.

Millimeter radio fluxes are low, smaller than 1 mJy. However, some pulsars demonstrate outbursts with higher fluxes. Therefore, the detection of a sufficiently bright outburst in the ground–space interferometer mode will for the first time enable resolving the light cylinder region (up to pulsar distances of several dozen kiloparsecs) and will provide invaluable information for understanding the nature of these objects and localizing the emission region of the observed electromagnetic radiation.

The angular size of the light cylinder is

$$\theta\,[\rm arcsec.\ s] = \frac{r_{\rm LC}}{d} = 3.2 \times 10^{-7}\,\frac{P\,[\rm s]}{d\,[\rm kpc]}\,,$$

where d is the distance to the pulsar. With an angular resolution of 40 nano arcsec, the light cylinder of a pulsar with a period of 1 s can be resolved from a distance of several kiloparsecs. An emission region size comparable to the light cylinder may additionally support the synchrotron model.

At the magnetosphere periphery, the magnetic field lines are bent due to plasma rotation, and a situation is possible where the emission generated at moderate altitudes above the neutron star surface cannot reach the observer, while the synchrotron radiation at millimeter wavelengths can be seen by the observer. In that case, the appearance of a pulsar seen only at millimeter wavelengths is possible (Fig. 11).

The search for and detection of pulsars generating only microwave pulses is a totally new field in pulsar studies, which can significantly increase the observed neutron star populations.

Studies of pulsars with the Radioastron ground–space interferometer suggest that there are interferometric responses exceeding the diffraction spot size, when the scattering circle of pulsar radio emission is resolved on the interstellar plasma inhomogeneities. Here, the amplitude of the interferometer signal does not decrease upon increasing the interferometer base to 240,000 km, the maximum length obtained by Radioastron for radio pulsar B0329 + 54 [82]. The structure of the interferometer signal with such long bases is related to the spectral parameters of the interstellar plasma inhomogeneities. For distant pulsars, diffraction scintillations can be observed at centimeter radio wavelengths. Observations of such pulsars by Millimetron in the interferometric mode jointly with the largest ground-based radio telescopes with 1 mln km bases will probe both the structure of the interstellar plasma inhomogeneities and the structure of the emission generation region in neutron star magnetospheres.

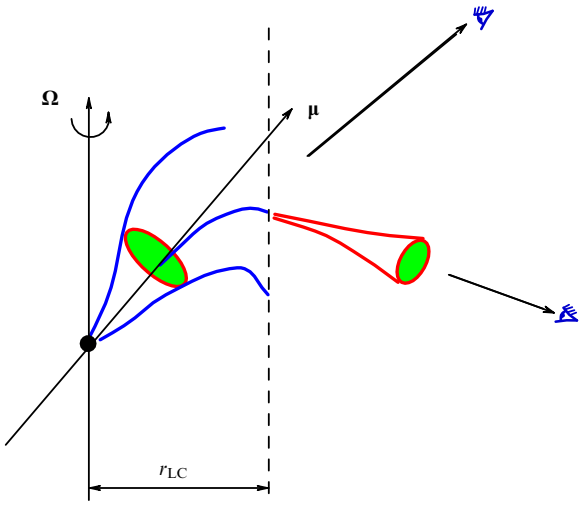

Figure 11. (In color online.) Pulsar emitting only at millimeter wavelengths. The magnetic field lines are shown in blue. The dashed curve shows the light cylinder, the emission regions are shown in green. The upper observer sees the radio emission in the meter, decimeter, and centimeter wavelengths, and the bottom observer receives only the millimeter radiation.

4.3 Relativistic objects in the centers of globular clusters

Single-dish mode observations of the central parts of the most massive globular clusters, in particular, with large core radii can be used to detect millimeter emission from stellar-mass black holes in binary systems. As soon as the signal is detected, observations in the ground–space interferometer mode with high angular resolution can be performed.

Black holes with masses $(5-20)\,M_\odot$ are end products of stars with masses $\geqslant 25 M_\odot$ in the main sequence [83]. Recent theoretical studies suggest that several hundred stellar-mass black holes can be present in old globular clusters [84]. Almost all of them should be single black holes, which is in agreement with the small number of X-ray sources with black holes in globular clusters. The presence of black holes can heat up the central parts of the clusters, leading to a significant increase in the cluster core radius [85]. Therefore, old globular clusters with large core radii are most suitable for searches for stellar-mass black holes.

Recent observations with the VLA (Very Large Array) discovered two black hole candidates in two globular clusters M22 [86] and M62 [87]. Both these clusters are massive, but they have different structures. For example, cluster M22 has an extended core, in line with theoretical predictions, while cluster M62 has a rather compact dense core.

VLA observations of M22 with the maximum possible angular resolution $\approx 1''$ revealed that the observed faint source can be in a binary system (Fig. 12a) with properties similar to those of stellar-mass black holes (Fig. 12b).

VLA observations of globular cluster M62 with a maximum time exposure revealed the presence of a very faint central source M62-VLA1 with a flat radio spectrum and radio flux 18.7 ± 1.9 μJy at the frequency 6.2 GHz [87]. The observed properties of this source in the radio, X-ray, and optical ranges are similar to those of the well-known transient X-ray source V404Cyg, which is believed to be a

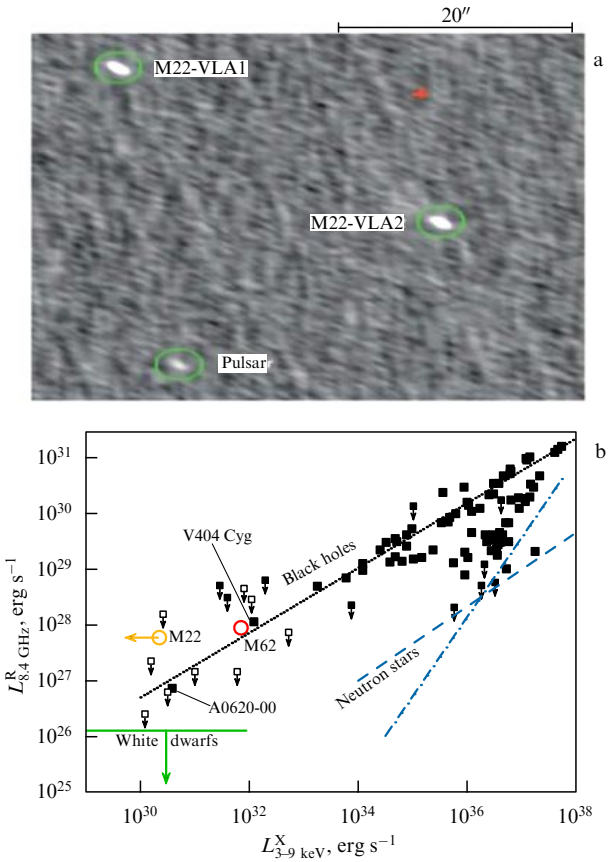

Figure 12. (In color online). (a) VLA image of globular cluster M22 in the continuum emission from the core. The two bright oval objects are sources identified as M22-VLA1 and M22-VLA2. The red cross shows the photometric center of the cluster [86]. (b) X-ray — radio flux relation from stellar-mass black holes. $L^{R}_{8.4\ GHz}$ is the radio luminosity at 8.4 GHz, $L^{X}_{3-9\ keV}$ is the 3–9 keV X-ray luminosity. The sources in M22 and M62 have properties rather similar to those of black holes and not of white dwarfs or neutron stars [87].

(presently quiescent) stellar-mass black hole in a close binary system.

High-sensitivity millimeter observations with moderate angular resolution of the black hole candidates discovered in globular clusters can be extremely important for confirming their nature. Assuming a flat radio spectrum, the expected millimeter fluxes from these sources can be a few μJy, while the fluxes from other stars should be much smaller. The main problem here is the separation of sources from the confusion background due to distant galaxies. Possible globular clusters to be observed include M22, M14, M53, M62, and NGC2419.

4.4 Origin of ultraluminous X-ray sources

The search for intermediate-mass black holes can be another exciting task. Observations of possible millimeter and submillimeter emission from ultraluminous X-ray sources (ULXs) and hyper-luminous X-ray sources (HLXs) in other galaxies in the single-dish mode with possible subsequent high-resolution observations in the ground–space interferometer mode should constrain the models and can help to unveil the nature of these sources.

Ultraluminous X-ray sources are off-center point-lie objects with the observed bolometric luminosity L exceeding the Eddington limit for galactic stellar-mass black holes ($20M_{\odot}$), $L > 3 \times 10^{39}$ erg s^{-1}, in the 0.3–10 keV energy range. ULXs were discovered in nearby galaxies by the Einstein X-ray observatory [88]. For a spherical accretion of fully ionized hydrogen, the Eddington limit can be expressed as [89]

$$L_{\rm Edd} = \frac{4\pi c G M m_{\rm p}}{\sigma_{\rm T}} \approx 1.3 \times 10^{38} \left(\frac{M}{M_{\odot}}\right) [\text{erg s}^{-1}],$$

where $\sigma_{\rm T}$ is the Thomson scattering cross section, c is the speed of light, G is the gravitational constant, $m_{\rm p}$ is the proton mass, and M is the black hole mass. This implies that ULXs can harbor intermediate-mass black holes, $M = 10^2 - 10^4 M_{\odot}$ (see, e.g., [90]). They can also be close binary systems at an evolutionary stage that is not observed in the Milky Way. The number of ULXs is quite high: 230 [91]; in addition, more than 500 ULX candidates have been discovered [92]. These objects are found in almost a quarter of galaxies [93] of all types: in star-forming galaxies (which contain about 60% of all ULXs) [94]; in dwarf galaxies (Holmberg II); in elliptical galaxies with low star formation rate, as well as away from star formation regions (NGC 1313 X-2 and NGC 4595 X-10) [95].

Immediately after the discovery of ULXs, different models of their origin were proposed. These models can be conventionally separated into three main classes: subcritical accretion onto an intermediate-mass black hole [96], supercritical accretion onto a stellar-mass black hole [97], and collimated emission from a stellar-mass black hole accreting at about the Eddington limit [98]. Because ULXs with different properties are observed, it is quite possible that the ULX population includes different types of objects. Stellar-mass black holes are the most likely candidates, and intermediate-mass black holes can explain the observed properties in several exceptional cases [99].

It is important to note that the existence of intermediate-mass black holes is an unsolved problem in astrophysics. Until recently, there has been no direct observational evidence of their existence and moreover no indirect indications of their reality, despite the predictions of the modern theory of structure formation in the Universe. Thus, intermediate-mass black holes are a missing link between stellar-mass black holes and supermassive black holes located in galaxy centers. According to current models, intermediate-mass black holes could be formed during collapses of primordial stars in the Universe, during the collapse of dense cores of young stellar clusters [100], as well as a result of accretion or stellar-mass black hole merging. In the last decades, indications of the presence of intermediate-mass black holes in the centers of globular clusters and in star-forming regions have emerged.

Unresolved central parts of massive globular clusters and HLXs are the most likely intermediate-mass black hole candidates. In one of the most probable intermediate-mass black holes, ESO 243-49 HLX-1, discovered by the XMM (X-ray Multi-Mirror Mission) Newton space observatory in 2004 in the spiral galaxy ESO 243-49 8 arcseconds from its nucleus [101], radio observations by ATCA (Australia telescope Compact Array) revealed variable radio emission at 5 and 9 GHz [102].

Radio emission has been discovered from some nebulae around ULXs. The best-studied examples are Holmberg II X-1 [103] and NGC 5408 X-1 [104]. Both show optically thin synchrotron radio emission, similar to radio emission from supernova remnants. Different radio sources show different

morphologies, but in some cases they look like binary sources [95].

Millimeter-range observations of the nearby ULXs with a sensitivity of ~ 1 μJy can provide more detailed information needed to estimate the black hole masses.

An unexpected result was recently reported by the NuSTAR (Nuclear Spectroscopic Telescope Array) observatory [105]. One of the ULXs in galaxy M82 turned out to be an X-ray pulsar ($P_{\rm pulsar} = 1.37$ s) in a binary system with an orbital period of 2.4 days. The mass function of the X-ray pulsar is $f(m) \sim 2M$. Most likely, this is a neutron star with a powerful magnetic field with strongly nonspherical magnetically collimated accretion onto accretion columns near the neutron star surface.

4.5 Supernovae

For several days after a supernova explosion, its remnant is very compact. One of the most plausible mechanisms of supernova explosions is the magneto-rotational mechanism [106–108]. In this mechanism, the explosion asymmetry arises due to the breaking of the magnetic field mirror symmetry [109]. Early observations of a supernova remnant can be used to measure the initial explosion asymmetry before the interaction of the remnant with the surrounding medium significantly affects particle trajectories of the expanding remnant. The Millimetron space observatory in the ground–space interferometer mode will be capable of resolving supernova remnants up to a distance of 10 Mpc. The expected number of events is several dozen per year for type-II supernovae and one per year for type-Ib/c supernovae.

Type-IIn supernovae could also be interesting for Millimetron observations. Such supernovae can be related to a common envelope stage in the massive close binary evolution [110, 111, 112]. The common envelope leads to asymmetric outflow of the external parts of a red supergiant. The shock wave propagation along the expanding red giant atmosphere can be observed in the millimeter wavelength range. In this model, the outflow asymmetry can be detected starting from the second day after the explosion for a supernova located at distances longer than 30 Mpc.

5. Black holes and jets

Black holes are one of the most intriguing predictions of general relativity, and the problem of proving or refuting their existence is a major task in astronomy. Black holes are extremely compact objects, and observing them requires a very high angular resolution. For all currently known objects, the angular size of the black hole horizon is less than 20 micro arcsec. Progress in this field, hopefully, will bring the answer in the near future. For example, the ground–space interferometer Radioastron with a record angular resolution of 7.5 micro arcsec is already carrying out observations of the supermassive black hole in the center of M87 galaxy. The ground-based EHT, operating in the millimeter range, will possibly resolve the central black hole in the Galaxy.

The Millimetron space observatory, operating jointly with ground-based telescopes, will enable measurements with an ultrahigh angular resolution and will therefore be capable of probing smaller physical scales and a larger number of objects beyond these two nearby black holes. In addition to supermassive black holes, stellar-mass black holes in binary systems will be observed. These observations will help to probe the conditions of ultra-high-energy particle generation and of jet formation in the vicinity of black holes.

The VLBI specifics were taken into account when planning Millimetron's work. We assume that such an interferometer can be used to estimate the angular size of sources with ultrahigh angular resolution at submillimeter wavelengths, and with the corresponding sensitivity (see Table 1) to construct maps in the framework of a priori model assumptions on the source structure. The interferometer can also be used to construct one-dimensional intensity maps.

Critically important information on the magnetic field and nonrelativistic particle number density in the vicinity of nearby black holes can be obtained not only in the VLBI mode but also by polarization spectral measurements in the single-dish mode. The presence of a magnetic field in the plasma along the line of sight results in the Faraday effect of rotation of the polarization plane of linearly polarized light. This effect is qualitatively characterized by the rotation measure (RM), which is φ/λ^2, where φ is the angle of rotation of the polarization plane and λ is the wavelength.

According to theoretical studies [113, 114], the magnetic field on the scale of a black hole accretion disc can be $\geqslant 10^4$ G. Experimental papers [115, 116] showed that the magnetic field indeed increases toward the source nucleus. Therefore, if there are thermal electrons in the near nuclear region, an extremely large RM value can be expected.

Under quite reasonable assumptions on the magnetic field value and the thermal electron density, it is easy to estimate that RM $> 10^4 - 10^8$ ram m^{-2}. The latest results confirm theoretical predictions of the extreme values of RM both from the galactic center [117, 118] and from distant active galaxies at millimeter wavelengths [119]. For linearly polarized synchrotron radiation from the nuclear region, narrow-band frequency channels of the Millimetron detectors will observe 'sine-like' variations of the radiation flux density as a function of wavelength.

Detection of the extreme Faraday rotation by ground-based telescopes or by Millimetron in the single-dish mode will provide a list of candidate sources with definitely small angular sizes, which can subsequently be observed by Millimetron in the interferometer mode.

The origin of supermassive black holes in galactic nuclei is discussed in Sections 7.3 and 7.6.

5.1 Nearby black holes

Almost all nearby supermassive black holes (at distances less than 50 Mpc) have a luminosity below the Eddington limit, which is related to comparatively weak accretion. Notably, these black holes include the black hole in the Milky Way center (Sagittarius A*), M87, and Centaurus A.

When modeling such sources, the accretion rate is assumed to be many orders of magnitude smaller than the Eddington value. For such small accretion rates, the standard disc accretion theory is inapplicable, and the so-called advection-dominated and radiative-inefficient models are under study. In these models, the accretion disc near the black hole is assumed to be geometrically thick, with the characteristic thickness of the order of the radial distance to the black hole. Because the dilute plasma of the disc radiates ineffectively, the matter heats up and expands in the vertical direction. The gas temperature can be as high as $10^{11} - 10^{12}$ K, and most of the accretion energy released is advected by the radial inflow into the black hole. Therefore,

the efficiency of the released energy conversion into radiation is very small, typically of the order of $10^{-6}-10^{-3}$.

Because the accreting plasma is quite dilute, the optical depth for free–free processes and Thomson scattering is believed to be small. Moreover, in the submillimeter range, it is possible to neglect the synchrotron self-absorption as well. This means that the medium near the black hole in the submillimeter range is optically thin, and the black hole can be directly observed. Therefore, it becomes possible, in theory, to determine the black hole mass, angular momentum, and parameters of the accreting flow and its geometrical structure. With a sufficiently high angular resolution and high sensitivity, it can be possible to directly observe jet formation and matter outflow in such flows, and thus to shed light on the so far unsolved problem of whether the jets result from magneto-hydrodynamic processes in the disc or arise due to the so-called Blandford–Znajek effect related to fast rotation of the black hole. If scales smaller than the gravitational radius can be probed, there appears a very important possibility to study turbulence of the accretion flow and to understand the related phenomenon of quasiperiodic luminosity oscillations, which, for example, can be due to the presence of hot spots in the disc and/or the excitation of different oscillation modes in the accretion flow by turbulence.

The best-studied object like this in the Galaxy is Sgr A* (Fig. 13). The distance to this black hole is $R \approx 8$ kpc, its mass is $4 \times 10^6\, M_\odot$, the gravitational radius is $r_g \approx 10^{12}$ cm, the bolometric luminosity is 3×10^{36} erg s^{-1}, and the angular size of the horizon is $r_g/R \approx 10$ micro arcsec. The variability time scale is from several minutes to several hours in the near-infrared, X-ray, submillimeter, and millimeter ranges.

There are several breakthrough tasks for Millimetron in the astrophysics of black holes. The primary task is to resolve the gravitational radius for almost all supermassive black holes within 50 Mpc. The Millimetron space observatory will in principle be capable of resolving the structure of accretion flows around black holes at scales of the order of the gravitational radius for about 40 supermassive black holes. For objects such as the supermassive black holes in the galactic center or in M87, the angular resolution of Millimetron will be sufficient to study details that are fractions of a percent the size of the gravitational radius (Fig. 14). This allows probing turbulence in the surrounding gas flows, which is a major problem in any accreting source.

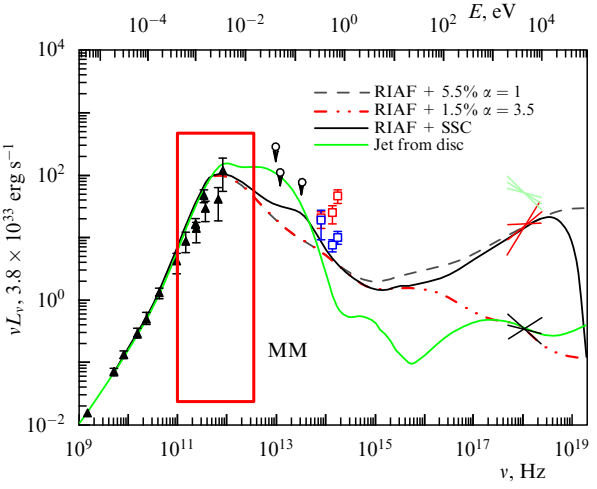

Figure 13. (In color online.) The spectrum of the galactic center (http://www.mpe.mpg.de/368843/Results). Radiatively inefficient accretion flow (RIAF) with the fraction (in percent) of nonthermal electrons with a power-law spectrum characterized by the slope q. SSC (Synchrotron Self-Compton) model takes Compton scattering of synchrotron photons into account. The symbols show radio and IR measurements; the crossing segments show the X-ray spectral measurements. The red quadrangle shows the Millimetron range.

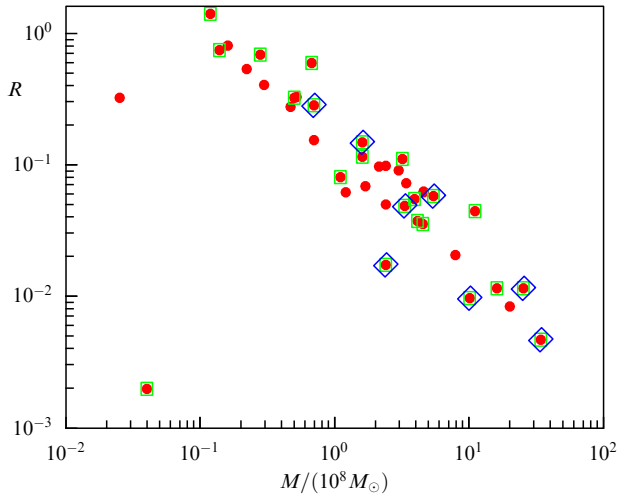

Figure 14. (In color online.) The ratio of the minimum angular size that can be resolved by Millimetron to the gravitational radius for 38 supermassive black holes at distances within 50 Mpc. The minimum angular size is assumed to be 2×10^{-13} rad. Filled circles correspond to the sensitivity threshold 10^{-4} Jy in the interferometer mode, filled squares correspond to 10^{-2} Jy, and diamonds correspond to 10^{-1} Jy. The square in the bottom left corresponds to the central black hole in the Galaxy; the bottom right diamond shows the black hole in M87 [120].

5.2 Shadows of black holes

As noted in Section 5.1, if the gas near a black hole is optically thin, and the black hole can be seen directly. Indeed, some radiation of this gas is captured by the black hole, and hence the region around the black hole should appear at large distances as a dark spot corresponding to the captured radiation. The brightness distribution around this spot changes very strongly due to strong distortion of the light trajectories near the black hole, gravitational redshift, etc. The brightness distribution around the dark spot can be used to study the main characteristics of the emitting gas, for example, to determine whether the disc or the jet makes a dominant contribution to the object luminosity at a given wavelength. The shape of the brightness distribution around the dark spot is also strongly dependent on the black hole spin, and the study of this region is apparently the most direct means to determine this fundamental parameter. However, the most significant issue is that the discovery of the black hole shadow would be direct evidence that the superdense and supermassive object in the center of the galaxy under study is indeed a black hole. The angular resolution of ground-based interferometric systems is limited by Earth's diameter, and generally is sufficient only to search for shadows around two of three of the closest supermassive black holes, whereas observations from Millimetron in the interferometer mode offer the fundamental possibility of discovering shadows around several dozen such objects (see Fig. 14).

Figure 15 shows the expected shapes of shadows from the central black holes in our Galaxy and M87, which were calculated numerically. In Fig. 15a, the black hole illumina-

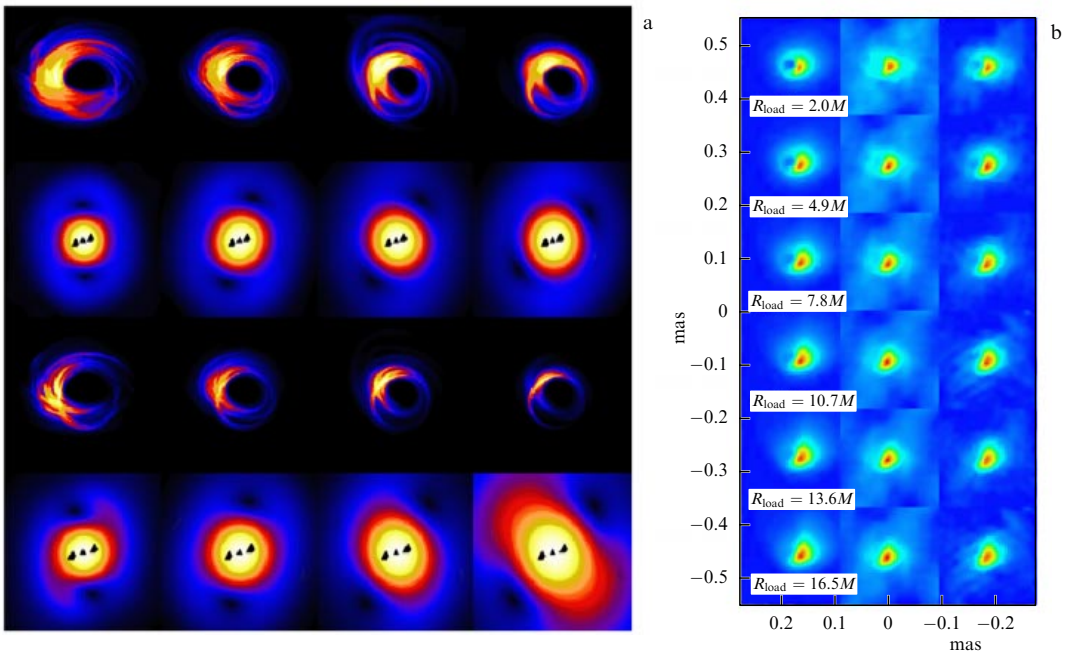

Figure 15. (In color online.) (a) Model image of a radiatively ineffective accretion disc and shadow from the central galactic black hole. Shown are the intensity distribution (1st and 3rd rows) and the visibility function amplitudes (2nd and 4th rows) for different models of the accretion flow (in different columns). The models differ by the black hole spin parameter (from left to right): 0.50, 0.90, 0.92, 0.94. The upper and bottom two rows are calculated for the respective wavelengths 1.3 mm and 0.87 mm [121]. (b) The brightness distribution of the central region of galaxy M87. The black hole is assumed to be 'illuminated' by a jet. Calculations are done for the frequency 345 GHz. The left column shows the initial model distributions, and the center and right columns show the model interferometric images obtained by different methods. M is the black hole mass. Geometrical units with $G = c = 1$ are used. The physical units are obtained by multiplying the mass by G/c^2. The jet formation radius from the black hole decreases from bottom up [122].

tion was due to a radiatively ineffective disc, and in Fig. 15b is due to a jet. The calculations were carried out taking the parameters of the EHT telescope into account. It is very important to perform similar calculations for parameters of the Millimetron space observatory.

5.3 Remote black holes

Millimetron will offer the possibility of resolving the gravitational radius of a black hole with a mass of 100 mln solar masses located at a distance of 100 Mpc and for a black hole with a mass of 1 bln solar masses from a distance of 1000 Mpc. Many bright active galactic nuclei and quasars can be found at such distances, which presumably contain black holes in this mass range, with the accretion proceeding through the standard geometrically 'thin' accretion disc. The presence of such a disc can be inferred from a 'Big Blue Bump' in the UV spectrum. Although discs around these black holes can be optically thick, the shadows of black holes can also be sought here (Fig. 16) because the size of such discs in the direction perpendicular to the disc plane is rather small compared to the horizon angular size.

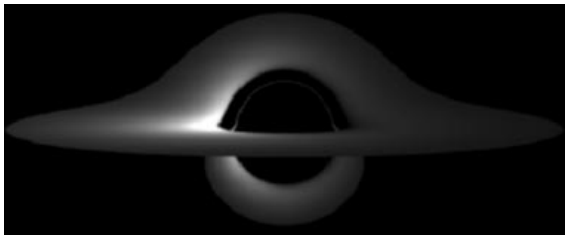

Figure 16. The bolometric flux distribution from an accretion disc around a Schwarzschild black hole. The disc inclination angle to the line of sight is 84.5° [123].

At long distances, it is also possible to observe very interesting nonstationary phenomena in active galactic nuclei and quasars, which are not observed in relatively close objects due to low probability. We briefly discuss only two phenomena: the process around supermassive binary black holes (SBBHs) and tidal disruptions of stars by a supermassive black hole.

The SBBHs not only are interesting objects in and of themselves but also can generate the most powerful bursts of gravitational radiation during coalescence, which can, theoretically, be observed by future space gravitational wave interferometers from very large distances (up to cosmological scales). Apparently, the best-known SBBH candidate is the BL Lac object OJ 287 located at a distance of 1 Gpc. OJ 287 is thought to be an SBBH with component masses of 10 bln and 100 mln solar masses and an orbital period of 12 years (Fig. 17). In this case, Millimetron can easily resolve the scale of the order of the angular size of the horizon of the more massive component.

Tidal disruptions of stars by a black hole are usually manifested as X-ray outbursts in inactive galactic nuclei. The characteristic decay time of the outbursts is about a few years.

If the submillimeter luminosity of these objects is sufficient to be observed by Millimetron in the interferometer mode, estimates show that Millimetron will be capable of resolving scales of the order of the gravitational radius at least for several objects, including NGC5905 [124]. A very interesting source, Swift J1644+57, discovered in 2011 [125] and located at a distance of about 1 Gpc, is very powerful at all wavelengths, including the millimeter range. This source is interpreted as a jet formed after the tidal disruption of a star

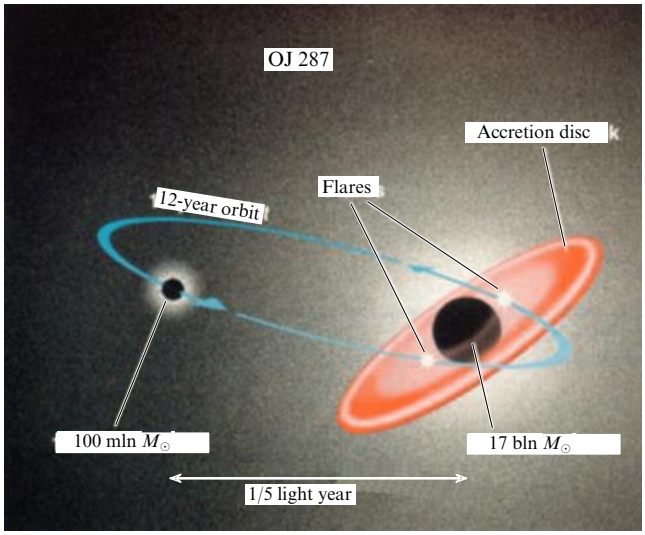

Figure 17. Possible schematic of OJ 287 (http://www.astro.utu.fi/news/080419.shtml).

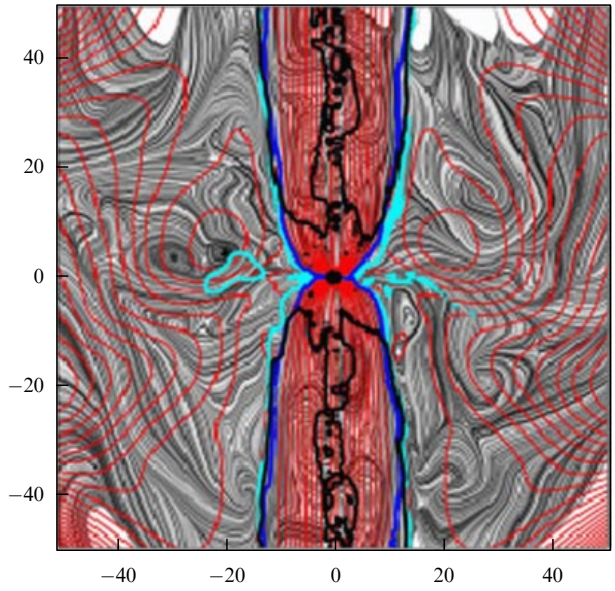

Figure 18. (In color online.) Velocity and magnetic field distributions in the jet (respectively shown in grey and red) according to the relativistic jet formation model near a black hole with the spin parameter $a = 0.9375$ [130]. The axes show the coordinates as multiples of the Schwarzschild radius of the black hole.

by a black hole. Millimetron will be able to test the origin of such events.

5.4 Physics of jets

The variety of accretion theories results in a variety of theories of jets. As in the case of discs, the Millimetron space observatory, thanks to its record parameters, will provide missing observational data needed to test different models.

The main problems of the physics of jets in systems containing supermassive black holes can be listed as follows (see, e.g., [126]). First, it is necessary to understand the jet formation mechanism — either due to black hole rotation or due to the accretion disc. Second, to understand the jet's origin, the magnetic field structure near the black hole should be known. Third, it is still unclear what kind of plasma moves in the jet (electron–positron or electron–ion), what its characteristic velocity is as a function of the distance to the black hole and to the jet axis, what the distribution of nonthermal particles in the jet is, etc. Fourth, it should be reliably determined whether 'typical' jets are two-sided or one-sided (i.e., whether the formation of a jet directed to only one side is possible) [127]. Fifth, it is important to obtain observational confirmation of the possible change of the jet magnetic field polarity [128, 129]. All these problems are interrelated.

In different numerical models, the very possibility of jet formation depends on the accretion disc structure and the magnetic field (Fig. 18). Clearly, to unveil the nature of jets, observations with high angular resolution are required, which can probe the matter outflow and the magnetic field structure around black holes. VLBI-mapping taking polarization into account can be hampered by extreme Faraday rotation. Possible methods of mapping are proposed in [131–134].

Jet formation studies are closely related to accretion disc studies, and observations of these objects in different types of astrophysical objects, from stellar-mass black holes to quasars, are crucial. With the record high angular resolution in the interferometer mode, Millimetron can possibly solve these problems. We stress that to study the magnetic field structure, polarization measurements are indispensable.

Finally, millimeter observations can be decisive in understanding the nature of GeV and TeV flares from active galactic nuclei [135]. Such flares are observed from galaxies M87 and 3C454.3 each 2–3 years and last from several days to several weeks. Ultrahigh angular resolution observations can both localize the flare in the jet and follow the evolution of the emitting region. To clarify the origin of the flares, it is also important to simultaneously observe the central regions of active galactic nuclei [127, 136–138].

5.5 Jets from cosmic gamma-ray bursts

The unprecedentedly high angular resolution of Millimetron in the interferometer mode offers the possibility of directly observing jets from cosmic gamma-ray bursts during the first several days after the burst, when the jet expansion is relativistic. Indeed, for gamma-ray burst GRB 030329, located at the redshift $z = 0.1685$, the angular resolution of 0.16 micro arcsec corresponds to 0.0005 pc, which is equivalent to the light time of 1 day. Thus, it becomes possible to observe and investigate the early phase of jet expansion, apparently even before the jet-break time, when the GRB afterglow power-law light curve shows a break.

These observations will substantially complete ground-based VLBI observations [139] and will allow determining several important parameters, such as the jet-break time, the time of jet deceleration, the time of the transition from relativistic to Newtonian expansion, as well as testing the possibility of the occurrence of two jets of different nature [140–142]. Nearby gamma-ray bursts are quite rare, once in 5–7 years, and it will hopefully be possible to detect one such event during the Millimetron mission lifetime.

6. Galaxies

6.1. Evolution of galaxies

Star formation leads to dust production; therefore, star-forming galaxies are bright sources in the submillimeter range. On the other hand, even warm dust ($T_d = 30$ K) in

early galaxies at redshifts $z = 10$ will be seen in the submillimeter range. The spectral line 158 μm of the CII ion, which provides the cooling of the interstellar gas with temperatures 30 K to several thousand K also falls in the millimeter wavelengths. This will make Millimetron, with its high sensitivity, a powerful instrument for detecting galaxies at high redshifts up to $z \sim 6-7$ and for drawing a sufficiently complete picture of the evolution of galaxies. For this, both continuum and spectral line (CO, CII, OI, etc.) observations are required. The angular resolution also plays a key role.

Galaxies with active star formation are so numerous that under insufficiently high angular resolution they can merge into a confusing background. For the Millimetron 10 m primary mirror, this effect is much weaker than for the Herschel telescope and the SPIC project with 3.5 m mirrors (Fig. 1b). Preliminary estimates show that Millimetron will be able to measure spectra of at least 10,000 galaxies and to make continuum observations for several tens of millions of galaxies. Thus, it will be able to obtain three orders of magnitude more information than the Herschel telescope. Millimetron will be able to defect light from galaxies with redhsifts up to $z = 6-7$ (Fig. 19).

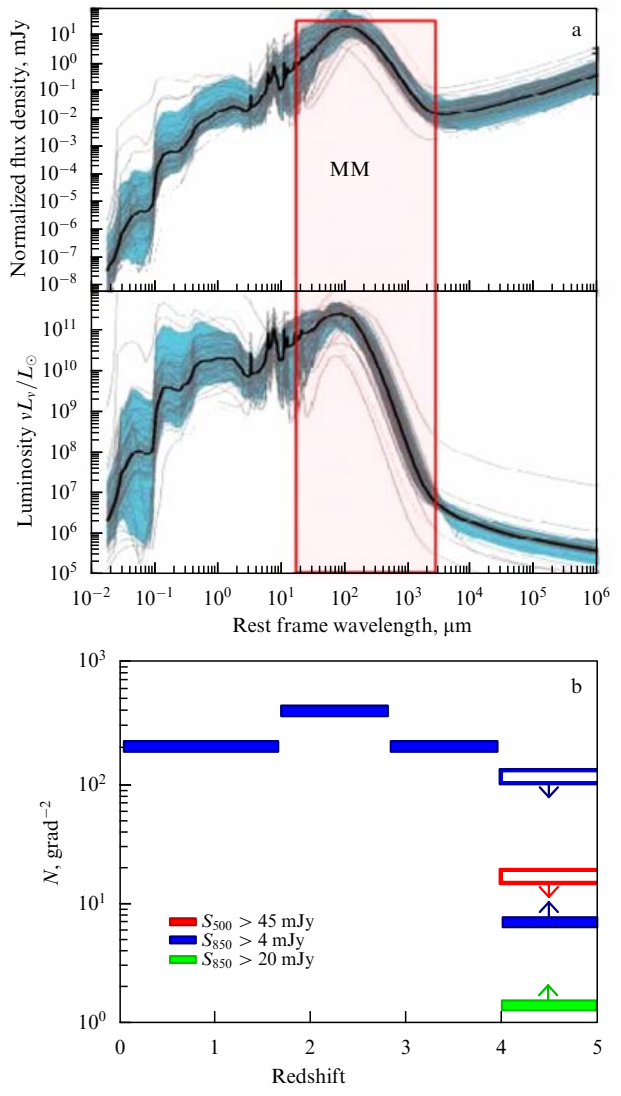

Figure 19. (In color online.) (a) Spectral energy distribution from typical submillimeter galaxies (in the rest frame) peaking at the wavelength $\lambda \approx 100$ μm [143]. The red rectangle shows the Millimetron operation range in the single-dish mode. (b) The distribution of the submillimeter galaxy number density as a function of redshift [144]. S_{500} and S_{850} are the fluxes at 500 and 850 μm.

Lyman-alpha emitting galaxies represent another very interesting aspect of galactic evolution studies. The source of emission in these galaxies and their place in the general scheme of galaxy evolution are still unknown. The problems to be solved include:

— what is the dust content in these galaxies;

— what evolutionary stage do they represent;

— what are the energy sources: accretion onto a black hole, stellar emission, or gravitational energy?

To answer these questions, photometric and spectral observations of these objects, identified by their optical emission, are necessary. Due to the high sensitivity, Millimetron can study typical objects with fluxes of several tens of μJy [145].

6.2 Regions with low star-formation rate

The outstandingly high sensitivity of Millimetron enables measuring the temperature and mass of the dust along the line of sight in the dilute galactic and intergalactic environment, where dust is found under the specific conditions of a low-density diffuse medium (an order of magnitude lower than near the Sun), and understanding the mechanisms responsible for the presence of dust and its heating. Studies of dust at the periphery of galactic discs, in elliptical galaxies, and in galaxy clusters, where the dust formation process is difficult, will allow clarifying the dust and gas transport into circumgalactic and intergalactic space and understanding the features of gas molecularization and the star formation character in low-density interstellar matter.

Recent studies have revealed two types of spatial dust distribution at galactic peripheries. In one case, the dust-to-gas mass ratio decreases with the radius proportionally to the metallicity decrease, as in galaxies M99/M100 [146] or M31 [147, 148]. In the other case, the dust-to-gas mass ratio remains nearly constant at distances up to one and a half optical radius, even though the underlying metallicity decreases outwards [149, 150]. The first case corresponds to *in situ* dust production, i.e., along with metals; the second case corresponds to radial selective dust transport out of the galactic disc or an overestimation of its relative content. This dichotomy in the spatial dust distribution at the galactic periphery (if confirmed) apparently reflects the features of dynamical processes in galactic discs, and can be of primary importance for galactic disc evolution.

Infrared radiation fluxes from dust at the periphery of galaxies suggest the dust temperature $\lesssim 20$ K (Fig. 20). The dust emission flux beyond the galactic disc radius, usually taken to be its photometric radius, is typically below the Herschel sensitivity; however, it should be sufficient to be detected by Millimetron. Addressing this task by Millimetron will allow:

- finding the source of dust heating in the ISM as a whole, at the periphery, and beyond stellar discs;
- clarifying optical properties of dust at the galactic periphery, which will help to understand the dust transport (or production) mechanisms far away from the main dust production sources;
- studying the gas-to-dust ratio as a function of the local star formation rate, the surface gas density, and its quantity. This, in turn, will give a new means to estimate the total mass

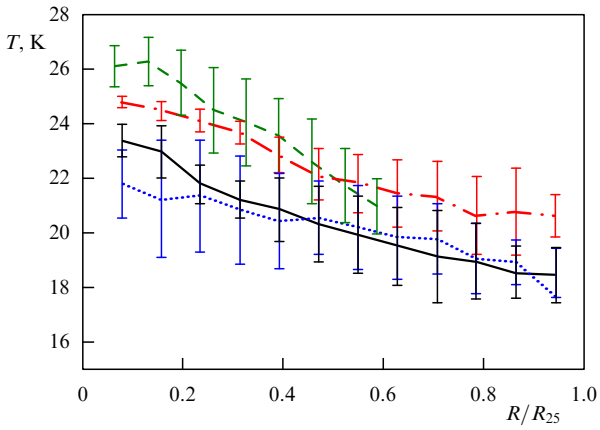

Figure 20. (In color online.) Radial variation of the dust temperature in four galaxies: NGC 4254 (red curve), NGC 4303 (green curve), NGC 4321 (blue curve), and NGC 4501 (black curve) [151]; R_{25} is the 25th magnitude isophote radius.

of molecular gas and to understand its role in the star formation process;

• evaluating the mass of dark molecular gas (not detected in CO lines due to dissociation of this molecule), which manifests itself via gamma-ray emission, the presence of dust, and ionized carbon emission [23, 152]. The low-density regions can contain most of the hidden molecular gas. The example of the Galaxy shows that the fraction of CO-dark molecular gas increases with decreasing gas density, reaching 80% at a distance of 10 kpc from the center [23];

• using the relation between the gas and dust content and density to determine the ISM spatial distribution and relate it to the observed star formation rate in low-density gas regions: at the far periphery of galactic discs [153], in tidal structures (tails and bars of interacting galaxies), and in the vicinity of interacting galaxies in the intergalactic space, where star-forming regions are also found [154]. Of special interest are studies of the faint dust emission in very low-surface-brightness spiral galaxies (such as Malin-1 and Malin-2) and in galaxies with a very low column density of HI in the disc, which, nevertheless, have a spiral structure and at least in some cases contain molecular gas detectable in CO-lines [155]. Faint FIR emission was registered only from a few such objects [156]. A dust mass estimate will determine the molecular gas content unobserved in CO lines and its spatial distribution in these objects, which is important to explain the spiral structure and low star formation rate in discs of these galaxies, as well as features of their evolution [157];

• performing a detailed investigation (which seems to be of fundamental importance) of FIR emission from star formation regions near interacting galaxies (in bridges and connecting bars as observed, for example around the Antennae galaxies or in the M81/M82 group), where a large amount of dust is found that can, in particular, affect gas thermodynamics and stimulate a star formation burst in the bar. In the gas bar in the M81/M82 group, the dust in extinction is observed with a dust-to-gas ratio six times higher than the standard value in the Galaxy [158]. Unfortunately, this region of the sky can suffer from the effect of Galactic Cirrus (clouds of a comparatively low surface density above the galactic plane), which complicates the correct interpretation of extinction measurements. Because the gas and dust temperature in bars is low, the Millimetron

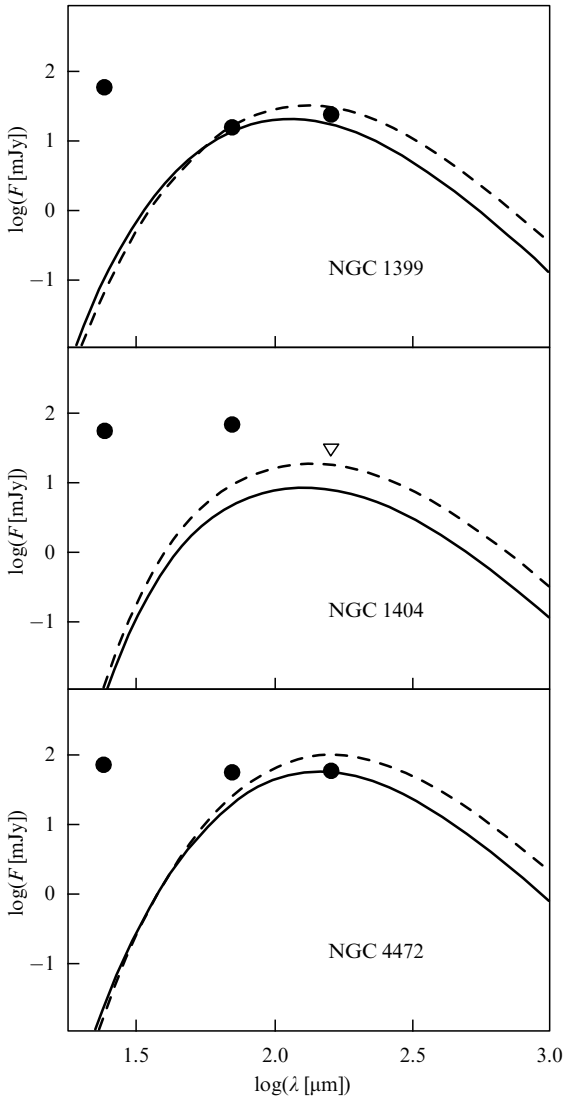

Figure 21. Comparison of fluxes F at 24, 70, and 160 μm (dark dots) for three elliptical galaxies with model spectral energy distributions [159]. Dust components with different temperatures are clearly visible.

observations could give a definite answer as to the amount of dust in the M81/M82 region.

Also of importance for the physics of galaxies are dust abundance studies — determining the mass, optical properties, and spatial distribution — for low-surface-brightness galaxies. This not only will provide estimates of the amount of CO-dark molecular gas, which is important for the correct dynamical modeling of such galaxies and their dark matter halos, but will also allow explaining the star formation mechanism under the conditions where standard criteria are not met. Infrared fluxes expected from low-surface-brightness galaxies are below the Herschel sensitivity limits, but should be measurable by Millimetron.

Elliptical galaxies with a low dust content and almost without cold gas constitute another interesting object for studies. The current data suggest that the dust is present there in the form of components with different temperatures (Fig. 21). Due to the low gas density, the dust in elliptical galaxies immediately finds itself in the hot gas phase and turns out to be subjected to the destructive effect of the hot gas. From this standpoint, elliptical galaxies are a unique

laboratory in which the dust destruction mechanisms must clearly show up. On the other hand, in the low-density conditions in elliptical galaxies, where the collision friction is weak, the dust transport by radiation pressure is clearly manifested; therefore, the emission of the space dust structure in these galaxies will help to understand the dust redistribution and its total 'budget' in the Universe.

Dust studies have another very important aspect: the dust is responsible for optical absorption, and hence the correct interpretation of many optical observations requires knowing the dust distribution. For example, this is of fundamental importance for the observations and interpretation of distant supernovae in projects to determine the cosmological constant (dark energy) [160, 161]. Different estimates are controversial, differing by several times [162, 163]. For example, an analysis of about 10^4 galaxy clusters from SDSS (Sloan Digital Sky Survey) at low redshifts (0.1–0.2) with all background quasars within 1 Mpc around the cluster center [164] suggests the mean extinction $A_v = 0.003 \pm 0.01$. A close result is obtained from the analysis of 90,000 SDSS background galaxies and 458 foreground galaxy clusters at redshifts up to $z \sim 0.5$ [165]. The corresponding mean mass dust fraction $\rho(\text{dust})/\rho(\text{baryons}) \sim 10^{-5}-10^{-4}$ is 0.1–1% of the Milky Way value. In this connection, the measured dust extinction in the intergalactic space is interesting (and intriguing): $0.03 < A_v < 0.1$ [166], an order of magnitude higher than in the gas in galaxy clusters. This fact, if true, suggests that either dust is supplied to the intergalactic space by field galaxies (i.e., galaxies that do not belong to clusters or groups), or a significant fraction of dust in galaxy clusters is unobservable (being apparently bound in dense cold clouds with small geometrical cross sections). Both possibilities are worth a careful investigation.

On the other hand, from the analysis in [167] of about 7000 clusters and groups from SDSS at low redshifts (0–0.2), the dust mass fraction $\rho(\text{dust})/\rho$ (baryons) was derived to be from 5% to 55% for clusters and groups, respectively, compared to the local (galactic) value. For galaxy groups, this high value is understandable because the gas temperature in the groups is below the critical limit of the effective dust destruction, but the higher dust concentration measured in clusters [164, 165] may suggest that the dust in clusters is protected from destruction by dense cold shells of the gas of cloud fragments that are expelled from galaxies together with the dust.

The situation is not completely clarified even when we move to IR observations in emission, although some hints as to the possible answer emerge: the Spitzer space telescope data at wavelengths $\lambda = 24$ and 160 μm from the Coma cluster direction, contrary to expectations, do not show emission above the noise level [168]. However, later observations by the Herschel observatory at wavelengths $\lambda = 100$, 160, 250, 350, 500 μm revealed dust traces in the vicinity of several dwarf galaxies with extended halos in the FIR by reliably demonstrating gradient flattening at long wavelengths. The extended FIR emission with a 'colder' spectrum at the periphery of elliptical galaxy M87, which was initially interpreted in terms of cold dust emission, was later identified with synchrotron radiation [169]. The example of the M87 galaxy shows that the FIR and millimeter spectra of extended discs of spiral and elliptical galaxies can be formed by a superposition of cold thermal dust emission and nonthermal emission from relativistic electrons that diffused in the periphery regions of such discs. From this standpoint, submillimeter and millimeter observations could be crucial, because the difference between the Jeans thermal dust spectrum and the power-law spectrum of relativistic electrons with a negative slope can manifest itself in these bands. In this connection, the latest results of cold dust observations in coronae and extended discs of nearby isolated galaxies M31 [147, 148] and M99/M100 (Fig. 22a) [146] and in dwarf galaxies from the Virgo cluster [169, 170] should be mentioned. Similar dust coronae around galaxies are well observed in the optical band [167].

Recently, much evidence has been found of the existence at low redsifts (0.1–0.4) of extended circumgalactic gas coronae (up to 300 pc in size) enriched with heavy elements up to almost the solar metallicity [171, 172]. The dust should be expected to be present in these coronae in the same proportion as metallicity. Taking into account that the gas temperature in the coronae is not very high, probably around 10^6 K [173], a significant dust fraction can be preserved. Therefore, dust observations in such coronae could provide valuable information on dust evolution during its transport into the intergalactic medium.

6.3 Extragalactic star-formation regions

Observations of star formation regions in dwarf galaxies similar to Holmberg II and DDO 053 require a higher angular resolution than that available with the Herschel space telescope, at least as high as 10–20 arcsec at wavelengths longer than 200 μm. To observe low-metallicity star-formation regions, the sensitivity level should be better than 1 μJy per bin. Such Millimetron observations would be unprecedented and can bring breakthrough results.

A high angular resolution in the near-IR range was attained by the Spitzer telescope. However, to fully describe the dust, a similar FIR angular resolution is needed. Observations of polycyclic aromatic hydrocarbons (PAHs), in particular, a study of their abundance depending on the ISM parameters in galaxies, can be a promising task. These observations will clarify the reliability of PAH emission as star formation rate indicators and will address PAH survival and organic species evolution in the ISM.

In individual galaxies and star formation regions, the PAH abundance correlates with metallicity (Fig. 23a); however, the nature of this correlation is unclear. The dependence of the PAH formation processes on metallicity in stars or molecular clouds and processes of their destruction in the ISM and star formation regions are considered as possible explanations. The problem is significantly complicated due to the lack of high-resolution observations (at least 10 arcsec) at wavelengths above 200 μm. Without these data, the analysis of the PAH content, i.e., their contribution to the total mass of the dust, is impossible.

The lines [CII] (158 μm), HD (112 μm), HeH^+ (149 μm, 74 μm) , H_3^+ (95 μm), and H_2D^+ (219 μm, 207 μm) are the most important ones for extragalactic star-formation regions. For example, Fig. 23b shows a Herschel space telescope image of the star-burst galaxy M82 in the ionized carbon line at 158 μm. It is seen that the low angular resolution enables studying the general distribution of emission across the entire galaxy but not the individual star-forming regions.

Observations from the Herschel telescope and from other millimeter observatories have revealed that dust is present even where its presence has not been assumed before: in elliptical galaxies, where the dust must have been destroyed, and at the periphery of disc galaxies far away from star-

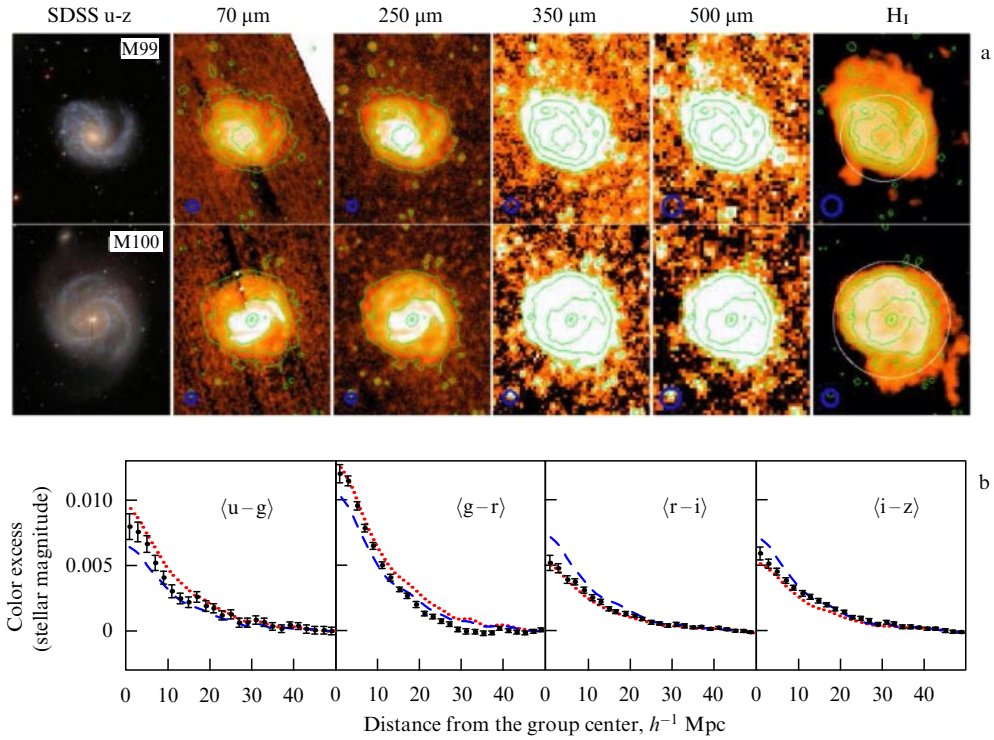

Figure 22. (In color online.) (a) Infrared and submillimeter emission from galaxies M99/M100 [146]: the increase in the disc size as the dust temperature decreases is clearly seen. (b) Extended dust coronae in galaxy groups [167]. h is the Hubble constant in units 70 km s^{-1} Mpc^{-1}.

formation regions. New high-precision measurements of the weak dust emission at the galactic periphery, as well as observations of protostellar and protoplanetary objects, are required to clarify these issues. The main method of research will be the spectral energy distribution measurements from these objects, with a high calibration accuracy being the key requirement that decreases systematic errors.

6.4 Dynamics of the interstellar medium and chemical evolution of the Universe

The chemical evolution of the Universe is of a fundamental nature and has philosophical meaning, because Earth and every living organism consist of heavy elements formed in the stellar interiors. Of profound importance are both the degree of homogeneity of chemically enriched matter [176, 177] and the homogeneity of the elemental abundance distribution. For example, from the standpoint of both the conversion of CO emission into the column density of H_2 molecules and the origin of life in the Universe, the key question is the precise carbon-to-oxygen abundance ratio, which can vary in space by an order of magnitude due to the chemical enrichment, depending on the initial mass function of supernova progenitors [178]. The basic observations of the chemical evolution of the Universe include measurements of the elemental abundance (the relative abundance of heavy elements), of the number density (mass fraction) of dust, and of variations in chemical composition due to dynamical phenomena, such as star formation and galactic wind.

The Herschel observations demonstrated a high capability of FIR observations to study heavy-element migration in the Universe. These observations include measurements of high-scale galactic matter outflows, such as galactic wind in M82 [175], and observations of bright infrared galaxies [179] and of dust migration in the galactic discs and at the galactic periphery (see the discussion in Section 6.2). The Herschel telescope results both provided new insights into the nature of the driving mechanisms of these matter flows and posed several new questions about their role in the dynamical and chemical evolution of galaxies and of the Universe (for discussions, see [175, 180]).

Thanks to the high angular resolution, Millimetron will be able to measure the difference in the chemical composition and elemental abundance of the interstellar gas on scales starting from heavy-element outflows from stars and supernovae. There are optical observations of relative elemental abundances in the Crab nebula that suggest that different elements show generally qualitatively similar but quantitatively highly different spatial distributions [181]. The angular resolution of the spatial variation scales is relatively low (about 10–15 arcsec); therefore, observations of the Crab nebula in the IR line [CII] at 145 μm with an angular resolution of 3–4 arcsec are of major importance for estimating the degree of inhomogeneity of the chemical abundance at the injection scales of heavy elements into the ISM. Similar observations with the same angular resolution are possible and interesting for other supernova remnants, for example, Cas A, as well as for nearby Wolf–Rayet stars. High angular resolution observations of the 158 μm and 145 μm lines are essential for studies of possible spatial separation of carbon and oxygen.

Using observations in the CO lines with high principal quantum numbers, as well as in the [CII] 158 μm and [OI] 145 μm lines and lines of other atoms and ions, Millimetron can study the ISM enrichment with heavy elements in detail. Observations of these lines in the direction of the assumed galactic fountains in the Milky Way — the local vertical outflows driven by collective supernova explosions in sufficiently massive OB associations [182] — are of great impor-

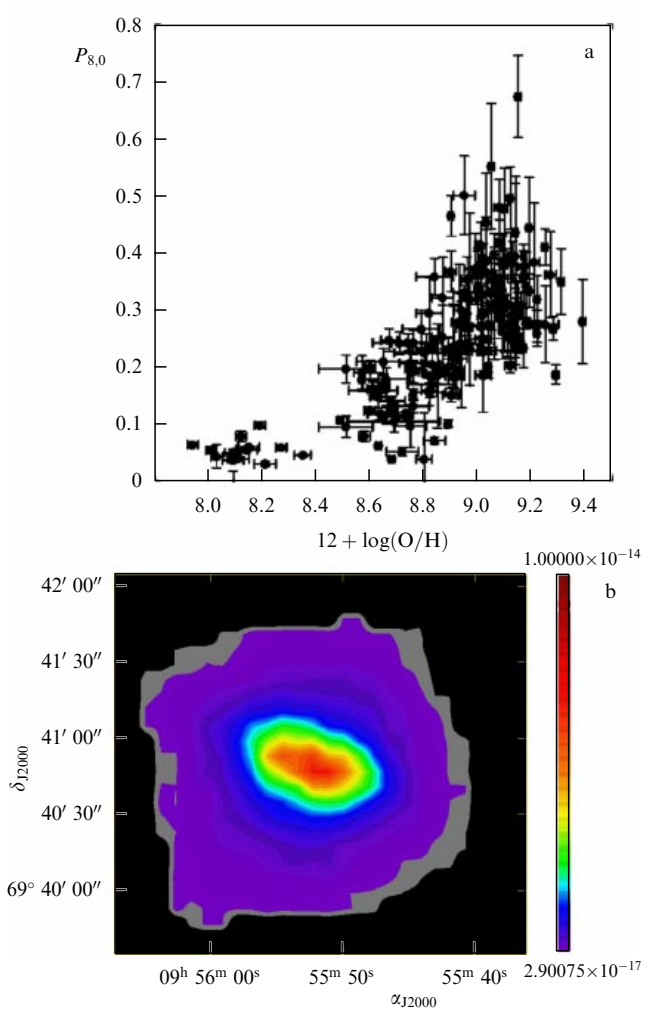

Figure 23. (In color online.) (a) Correlation of the intensity of PHC emission with metallicity according to observations of extragalactic star formation regions. The PHC emission is represented by the parameter $P_{8.0}$, the flux ratio at 8 μm to the total flux above 70 μm. To determine $P_{8.0}$, FIR observations with the same angular resolution as in near IR are needed [174]. (b) Image of galaxy M82 in the line of ionized carbon at 158 mm in celestial coordinates α, δ (epoch J2000) [175].

tance for studies of the chemical and dynamical evolution of the Galaxy because they can provide totally new information on the way heavy elements migrate from the galactic disc into the intergalactic medium and on their radial redistribution [183]. In the last few years, the heavy-element radial distribution in the Galaxy has been the focus of studies of the dynamical history of the Galaxy [184]. Recent important results here include a noticeable negative gradient of the C/O ratio [185] (change by a factor of three on scales from six to 12 kpc), which can reflect peculiarities in the chemico-dynamical evolution of the Galaxy [186].

A significant fraction (about a half) of heavy elements is confined in solid dust particles. Therefore, dust observations are of great importance not only from the standpoint of dust formation and its optical properties but also for studying the chemical evolution of the Galaxy. The detection of dust in spectra of distant quasars at redshifts $z > 6$ [187] revealed that dust can be formed in type-II supernova shells. Details of this process, as well as the amount of dust that can be produced by an individual supernova, remains obscure. Recent observations of the Crab nebula and of some historical type-Ia supernova remnants by the Herschel space telescope, have revealed the presence of a significant amount of dust in these remnants, which was produced and expelled during supernova explosions [188, 189]. However, reliable observational confirmations of the possibility of dust production by massive supernovae are still absent (see the discussion in [190, 191]). The possibility of observing emission from dust particles and their seeds in the submillimeter and millimeter range from massive supernovae in the local Universe, in particular in the Galaxy, would be of fundamental interest.

6.5 Gravitational lensing at high redshifts

Observations at high redshifts of dusty star-forming galaxies (DSFGs) will be carried out to study their evolution (redshift and luminosity determination) using homogeneous samples in the single-dish mode (photometric and spectroscopic millimeter observations).

Observations of the last decade significantly changed our understanding of the galactic evolution by demonstrating that bright dusty star-forming galaxies at high redshifts are about 1000 times more numerous than in the present-day Universe (see, e.g., [192]). Spectroscopic observations of 47 sources from the high-redshift galaxy catalog obtained by the South Pole Telescope (SPT) at 1.4 and 2 mm [193], carried out by the ALMA telescope in the frequency range 84.2–114.9 GHz, showed that the brightest DSFGs are gravitationally lensed sources [194]. Remote galaxies are lensed by the foreground galaxies in the strong gravitational lensing regime, giving rise to multiple images of the lensed galaxy. These results fully confirm the hypothesis on the gravitational lensing nature of DSFGs [195, 196].

Because studies of the properties and evolution of DSFGs are based on observations of bright lensed sources, the amplification coefficient must be known in order to determine the proper luminosity of the source. To estimate the amplification coefficient, the full geometry of the gravitationally lensed system should be known. For this, the following parameters should be measured: redshifts of the source and the lens, the relative positions of the lens and the source, the ratio of fluxes from the observed images, and the lens galaxy properties. The last are required in order to choose a proper model of the density distribution in the galaxy lens.

By the launch of Millimetron, large millimeter and submillimeter sky surveys by the Herschel telescope and SPT (220 GHz, 150 GHz) will have been completed. These surveys will be used to select the lensed DSFG candidates. The selected sample sources should meet the following main requirements: 1) the sources must have a thermal spectrum, because dust radiation in the infrared and millimeter ranges is produced due to the re-emission of absorbed short-wavelength photons emitted by stars; 2) sources with negative K-corrections, which are the first-order redshift correction to the wavelength, frequency band, and intensity, should be selected from the photometric data; 3) nearby IR sources with $z \leqslant 0.03$ (according to IRAS data) and radio-loud quasars with a flat spectrum, which also emit in the millimeter range, should be excluded.

Carbon monoxide (CO) lines are the most general indicators of the presence of molecular gas at high redshifts. The main observable CO transitions include $J = 1-0$, $2-1$, $3-2$, $4-3$, $5-4$, $6-5$. For example, the rest-frame emission frequency is 115.27 GHz for the transition CO $J = 1-0$, 576.3 GHz for the transition CO $J = 5-4$, and 691.5 GHz for the transition CO $J = 6-5$. The transition CO $J = 6-5$

produces the brightest line, indicating the presence of dense star-formation nuclei with compact morphology. For example, from a source at $z \sim 5$, the CO $J = 6-5$ transition is observed at 111 GHz. For sources with such redshifts, the [CII] emission line is shifted from 158 μm to 948 μm.

Undoubtedly, the ALMA telescope will complete most of the tasks by constructing the redshift distribution of DSFGs. However, the redshift range $z = 1.74-2.00$ is unobservable for ALMA [193]. In addition, ALMA can operate only within the atmosphere transparency windows, which complicates the construction of broadband spectra. In this respect, Millimetron has advantages in constructing broadband millimeter and submillimeter spectra.

In addition, it can be possible to solve the satellite problem in the ΛCDM (Lambda Cold Dark Matter) model by performing photometric observations of gravitationally lensed sources with anomalous image flux ratios and high-resolution spectroscopic measurements of high-redshift DSFGs in a wide frequency band.

The ΛCDM model predicts that large dark matter clumps (halos) that host large galaxies like the Milky Way should be surrounded by several hundred small dark matter clumps (subhalos) in which, seemingly, dwarf satellite galaxies should be located. However, only two to three dozen satellites have actually been found around the Milky Way. Moreover, the Milky Way satellite galaxies are not distributed spherically symmetrically, rather being confined within an elongated pancake tilted toward the galactic plane.

One of the possible solutions to the 'satellite problem' is observing gravitationally lensed systems with an anomalous image flux ratio [197], such as MG0414+0534, MG2016+112, H1413+117 [198]. Importantly, the source H1413+117 shows a significant flux (≈ 0.1 Jy) at a frequency of 1 THz (Fig. 24). In addition, the pixel lensing modeling of the gravitational lens JVAS (Jodrell/VLA Astrometric Survey) B1938+666 in the FIR revealed the presence of a satellite with a mass of $10^8\ M_\odot$ [200]. In this system, the source is a bright galaxy located at $z = 2.059$, the lens is a massive elliptic galaxy at $z = 0.881$, and an almost full Einstein–Chwolson ring with the diameter $\approx 0.9'$ is observed. The presence of a low-mass substructure, i.e., a luminous or dark satellite in the galaxy lens, must locally perturb the observed brightness distribution of the extended Einstein–Chwolson arcs. Because these arcs are formed by multiple images of the gravitational lens system, "surface brightness anomalies" can be found and analyzed using the pixel modeling technique and then used for gravitational detection and calculation of the mass and location of the substructure with a mass as small as 0.1% of the lens mass inside the Einstein–Chwolson ring [200].

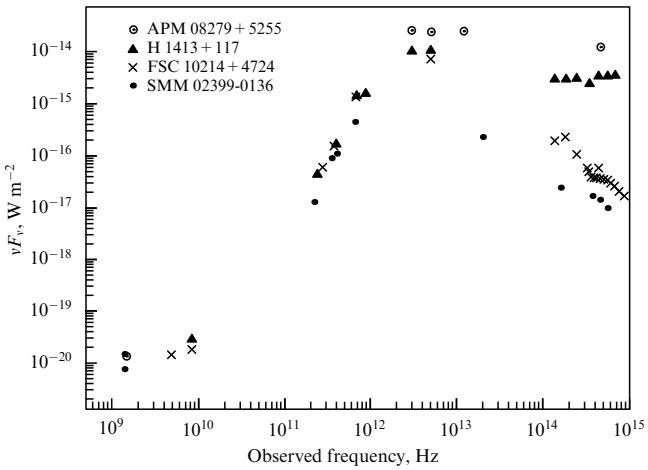

Figure 24. Broadband spectrum of gravitational lenses [199].

Another way to address the satellite problem can be high-resolution broadband spectral observations of high-redshift DSFG lensed galaxies. Large redshifts of the observed lensed sources allow obtaining a wide range of possible lens redshifts, which, in principle, can constrain the subhalo population evolution with redshift [201]. Here, of most interest are observations of the CO molecule transition $J = 6-5$, which is the brightest emission line and indicates the presence of dense star-forming cores with compact morphology.

A breakthrough task for the space interferometer mode is observations of gravitational lens candidates at high redshifts (up to $z \sim 5$) selected by submillimeter/millimeter observations in order to confirm the image multiplicity without mapping (an advantage of Millimetron), using only the visibility function for sources with a sufficiently high brightness temperature.

7. Cosmology

7.1 Infrared background and galaxy surveys

Galaxies at redshifts $z > 1$ have a maximum flux density at wavelengths $\lambda > 200$ μm and produce the cosmological IR background (Fig. 1a). Here, the capability of Millimetron to resolve more than 90% of the IR background into individual galaxies (Fig. 1b) can bring breakthrough results. The expected surface density of objects for photometric surveys is $\sim 10^5$ per square degree.

Massive spectral observations of a large number of galaxies will enable constructing three-dimensional catalogs of submillimeter galaxies at redshifts $z > 2$ and probing the evolution of the large-scale dark matter distribution when the Universe was less than three billion years old. Millimetron can complete 3D catalogs mentioned above by partially filling the gap between the recombination era (when the Universe was 300 thousand years old) and later epochs, up to the present time (when the age of the Universe is 3–13 billion years).

Studies of the 3D galactic space distribution, first of all, give invaluable information on the properties of galaxies themselves: by comparing cosmological numerical simulations with observations, it is possible to study the relation of the dark halo mass with the observed properties of galaxies [202]. This information is important for planning future cosmological tests from baryon acoustic oscillations, gravitational lensing, etc.

7.2 Cosmological angular distances

There are two main means of measuring the cosmological model parameters: geometrical and structural [203, 204]. The first method studies the Universe expansion law, from which its geometry and the equation of state of its constituents (matter, radiation, and dark energy) can be inferred. In this method, independent measurements of distances and redshifts of remote astronomical sources are required.

Long-term observations of water megamasers at a frequency of 22 GHz can be used to estimate the physical sizes of accretion discs by measuring the motion of individual

maser spots. The distances to these objects can then be derived from their angular size with quite high accuracy [205]. For ground-based interferometers with the maximum base, this distance is limited to 300 Mpc.

Interferometry with a superlong (cosmic) base can achieve an angular resolution better than 10 micro arcsec; therefore, a sufficiently bright source can be observed from any redshift. Such distance measurements as a function of redshift could allow probing the expansion law of the Universe and studying the dark energy equation of state with an unprecedentedly high accuracy.

However, this task requires multi-year, very high-precision observations, and therefore can be difficult to fulfill from Earth even for nearby objects. Presently, little is known about distant megamasers to reliably judge whether this can be done with Millimetron.

The same applies to another similar problem. The size of a black hole can be calculated from indirect measurements of its mass. The direct measurement of the black hole size can then be used to determine the cosmological distance. It is not clear as yet whether supermassive black holes in active galactic nuclei have parameters sufficient to be observed by Millimetron. This issue can be resolved after observations by the EHT or Radioastron telescopes of black holes in nearby galaxies and in the center of our Galaxy.

7.3 Distant galaxies and reionization of the Universe

The first stars (Population III) and galaxies must have been formed from primordial matter, not enriched with heavy elements. Observations of such sources are important not only for checking hypotheses on the formation of the first stellar objects in the Universe (which are the sources for reionization) at the first stages of the chemical enrichment of the Universe, details of the first galaxy formation, and peculiarities of star formation in the medium with the primordial chemical composition, but also for solving the supermassive black hole formation problem.

A galaxy enriched with heavy elements should emit in spectral lines of atomic and ionized carbon, carbon monoxide, oxygen, and other elements, and also in the continuum due to the presence of dust. Correspondingly, primordial matter should not radiate in the submillimeter range, except several spectral lines of the simplest molecules: HD at $112(1+z)$ μm, H_2 at $28(1+z)$ μm, and HeH^+ at $149(1+z)$ μm, where z is the galaxy redshift [15, 206, 207]. At the same time, atomic hydrogen emission should be observed in the near and middle IR band owing to high redshift.

The search for the first galaxies is one of the JWST tasks. The search includes studying the dependence of the number of galaxies on the redshift z: the vanishing of a number of galaxies at some z would indicate the galaxy-formation era. However, submillimeter and FIR observations are required to confirm the nature of such distant objects. The lack of the detection of dust and heavy-element atoms in the submillimeter range would suggest the discovery of a possible primordial galaxy. The final confirmation can be obtained through observations of the HD (56 and 112 μm) and H_2 (28, 17, 12, and 9.7 μm) molecular lines, which would indicate that gas cooling occurs without heavy elements.

The rotational lines of molecular hydrogen, as well as of its isotopic analog HD, provide the main outflow of the energy released during gravitational contraction of the first protostellar clouds. The fluxes in these lines can greatly exceed the sensitivity limit of Millimetron: ~ 0.1 mJy in the HD line at $112(1+z)$ μm [207] and ~ 1 mJy in the H_2 [207, 208] line at $28(1+z)$ μm, depending on the formation scenario of the first protostars. The detection of these lines is of primary importance, at least for determining the time of the beginning of star formation in the Universe. In addition, measurements of these lines will help to determine or improve the redshift of the first distant galaxies and quasars, which will help to construct a model of their evolution. Because the simplest hydrogen molecule is well studied, it is a good indicator of the physical conditions in the primordial ISM. Excitation conditions of the hydrogen molecule levels are also studied well, which enables probing physical conditions in the primordial gas.

The high sensitivity and availability of observations of molecular emission lines redshifted to the FIR is the main advantage of Millimetron in probing the physical conditions in the primordial gas. In the near future, only Millimetron will be able to study the relatively cold ISM ($T < 500$ K), including primordial gas cooling.

7.3.1 Spectral-space CMB perturbations. The 'dark age' epoch, when there were no stars or galaxies, ends by $z = 10-25$, when the first ionization sources appear: the first stars and galaxies, as well as black holes. The ionization of the Universe in this epoch can be both observed directly and inferred from CMB polarization studies [209, 210]. However, it is still unclear which potential ionization sources dominate. Observational studies of this problem will shed light on the formation mechanism of the first stars and supermassive black holes, whose mass can increase to $10^9\,M_\odot$ already by $z = 6$, i.e., during the first billion years of the existence of the Universe.

The reionization sources lead to the emergence of ionized volumes that can be probed by the kinematic Sunyaev–Zeldovich effect (the thermal Sunyaev–Zeldovich effect for these objects is much smaller). The expected level of spectral–spatial CMB fluctuations is $\Delta T/T = 10^{-7}-10^{-6}$, which corresponds to a flux of 1–10 μJy in the Millimetron band. The size of the ionization region is ~ 10 Mpc, corresponding to an angular scale of ~ 1 arcmin [211].

In addition, the emission from the HeH^+ molecule at redshifts $z = 20-30$ falls within the CMB range, which may cause the temperature fluctuations $\Delta T/T \sim 10^{-5}$ within the spectral bands $\Delta\nu/\nu \sim 0.01$ [212].

Spectral observations with low and moderate resolution in the 100–500 GHz frequency band can be used to analyze the form and evolution of ionized clouds and to formulate constraints on the reionization scenarios: whether Population III stars or supermassive black holes were the primary reionizaion sources.

7.3.2 Search for emission from the HeH^+ molecule. Searching for the HeH^+ molecule will help to understand the details of the interstellar and intergalactic media responsible for the formation of the first sources of ionization in the early Universe.

HeH^+ should be one of the most abundant molecules in the reionization epoch [213]. This molecule is formed in the primordial gas near powerful ionization sources. The rest-frame emission wavelengths are 149.1 and 74.6 μm. An exciting opportunity in the search for the HeH^+ molecule can be provided by observations of a quasar with $z = 6.42$ (and with the signal-to-noise ratio 3.5) (Fig. 25).

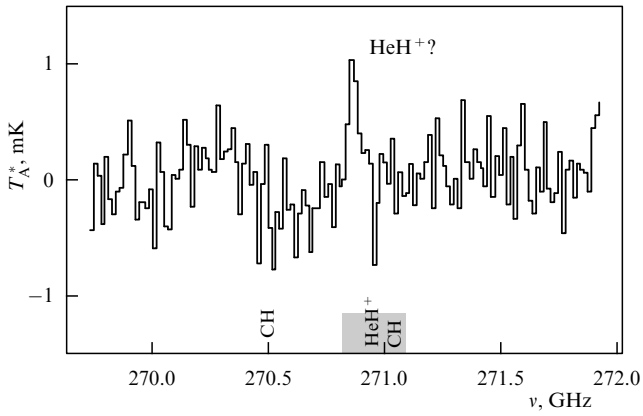

Figure 25. Spectrum of a remote quasar at $z = 6.42$ [214]. The signal-to-noise ratio ≈ 3.5 is insufficient to reliably detect the HeH^+ line.

7.4 Galaxy clusters

The CMB photons traveling through volumes filled with a sufficiently hot plasma experience spectral changes (Fig. 26). This is the essence of the Sunyaev–Zeldovich effect (SZ) [216, 217]. Galaxy clusters are the most appropriate for SZ effect observations.

Ground-based observations of the SZ effect are restricted by the atmosphere to frequencies below 300 GHz. The use of a space telescope may lead to a breakthrough related to the separation of the thermal SZ effect from other spectral distortions with sufficient accuracy (see Fig. 26), which can be used, in particular, to measure peculiar velocities of galaxy clusters (relative to the CMB). Measurements of these velocities will bring important information for testing and improving the cosmological model [203, 204].

Studies of galaxy clusters using the thermal and kinematic SZ effect will enable the measurement of the primordial cosmological power spectrum amplitude and the amount of dark energy in the Universe, and will help to study the growth of small perturbations and to obtain new constraints on the cosmological model, including the dark energy content. Using the SZ effect polarization, the CMB quadrupole amplitude can be measured from the standpoint of the observer comoving with the cluster, i.e., form different regions in the Universe.

7.5 Gamma-ray burst afterglows and host galaxies

Although more than 500 events have been detected in the optical band and more than 800 in the X-ray band since the discovery of gamma-ray burst afterglows in 1997, the most interesting spectral part of the afterglows remains poorly explored. Indeed, the maximum ν_m in the initial energy spectrum of an afterglow (Fig. 27) falls in the millimeter range. Afterglows that have been registered in this range [219] are shown in Fig. 28a. Observations of bright afterglows by Millimetron can constrain and in some cases determine the characteristic frequency of the synchrotron radiation ν_m and thus put stringent bounds on the energetic characteristics, parameters of the emission region, and the relativistic gamma-factor of the bulk motion of emitting electrons.

Presently, about 10% of the registered gamma-ray bursts have redshifts $z > 5$ [222]. However, the sample of high-redshift gamma-ray bursts is presently incomplete because of selection effects due to the difficulties in observing sources at $z \gtrsim 5$ (while the maximum redshift determined for GRB 090429B is $z = 9.4$ [223]), where the optical emission is effectively absorbed by the Lyα forest (Fig. 28a). Therefore, the sample of the currently observed distant GRBs represents at most 10% of the total amount of the sources. An intriguing issue is the discrepancy between the star formation rates inferred from distant galaxies and from gamma-ray bursts (Fig. 28b). The submillimeter observations of gamma-ray burst afterglows will increase the number of high-redshift sources. On the other hand, possibly some of the sources already observed are related to explosions of Population III stars [224, 225]. The redshift estimate $z \geqslant 15$ for at least one gamma-ray burst obtained from submillimeter observations could confirm the existence of Population III stars and their collapses producing gamma-ray bursts.

Of interest are optically dark gamma-ray bursts, in whose afterglows the optical-to-X-ray flux ratio is extremely small [226]. However, the redshift determination in such gamma-ray bursts is difficult due to low (or even zero) optical fluxes. Submillimeter observations of such gamma-ray bursts will help clarify their nature. Indeed, the absence of the host

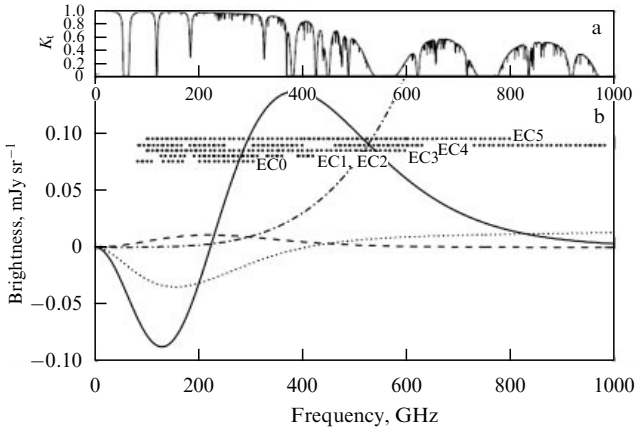

Figure 26. (a) Earth atmosphere transmission coefficient for a dry atmosphere. (b) The Sunyaev–Zeldovich effect spectrum (deviations from the blackbody CMB emission). The solid, dashed, dotted, and dashed-dotted curves respectively show the thermal effect, kinematic effect, effect on nonthermal electrons, and dust emission [215].

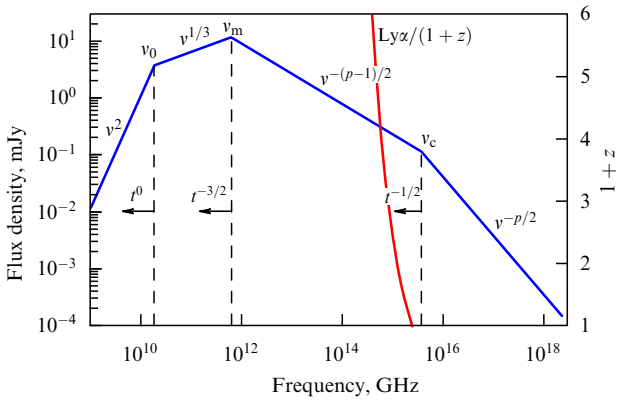

Figure 27. (In color online.) Theoretical spectral energy distribution of a gamma-ray burst afterglow [218]. The red curve shows the Lyα frequency in the observer frame as a function of redshift (on the right). To the right of this curve, the optical emission is suppressed due to absorption in neutral hydrogen along the line of sight.

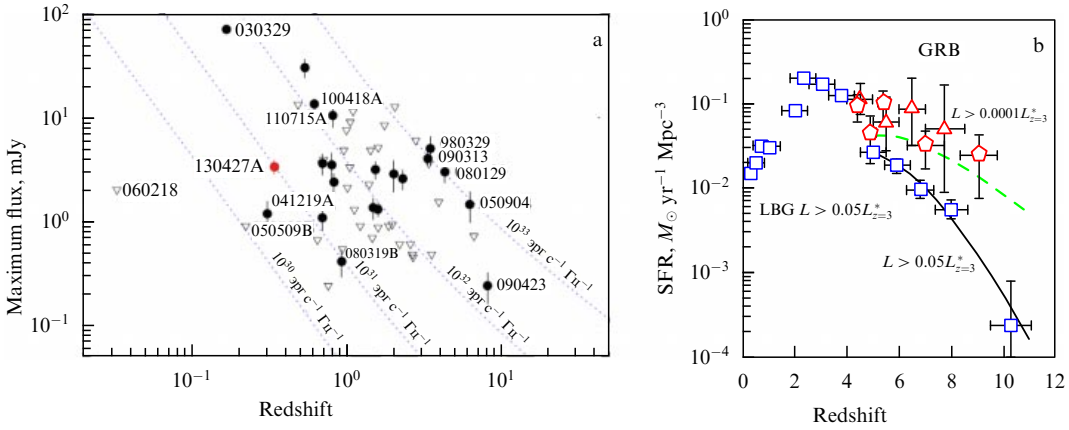

Figure 28. (a) Submillimeter gamma-ray burst afterglows [219]. Data for GRB 130427A are taken from [220]. The respective dark and light symbols correspond to detection and upper bounds. The dashed curves show the fluxes for sources with equal luminosity located at different redshifts. (b) The star-formation rate (SFR) as a function of the redshift z [221]. (GRB — gamma-ray burst, LBG — Lyman-break galaxy).

galaxy of a gamma-ray burst in the optical range (the most distant host galaxy presently known, GRB 100219A, has $z = 4.667$ [227]), and at the same time the detection of the submillimeter afterglow uniquely suggests a high redshift of the source. For close gamma-ray bursts, whose redshift can be determined by spectroscopic or photometric observations of the host galaxies, the detection of the submillimeter afterglow can be used to estimate the parameters of the absorbing circumburst medium [228–231].

7.6 Primordial black and white holes, wormholes, and the Multiverse

The most exciting problems of modern cosmology include: How was the Universe born? Are there other universes, and is it possible to obtain information about them? Today, this is a purely hypothetical field based on the analysis of GR equations [203, 232–238].

One of the least hypothetical assumptions is the formation of black holes in the early Universe. These black holes have a nonastrophysical origin and are referred to as primordial black holes. Their formation requires strong density inhomogeneities at the early stages of the Universe [239].

Primordial black holes can have a very wide mass spectrum and, depending on the mass, various methods are used to to search for them [240]. Millimetron will at least be able to study black holes with a mass higher than $10^4\,M_\odot$, both at the present time (see Section 4.5) and in the remote past, during the reionization of the Universe (see Section 7.3).

Features of the Universe passing through the singularity at the very beginning of the Big Bang can lead to the formation of interesting hypothetical objects — wormholes, relativistic objects similar to black holes but connecting different regions of space–time or even different universes (the Multiverse). Possible observational distinctions between black holes and wormholes include the presence in wormholes of a radial monopole magnetic field and radiation that brings information (the image, physical parameters, etc.) from different regions of our Universe and even from other universes [241–246]. Observational tests of this hypothesis will be carried out jointly with all black hole studies (see Section 5).

General relativity also allows solutions in the form of white holes [247, 248]. Such objects can be probed, for example, by explosions like anomalous gamma-ray bursts without host galaxies [249]. Searches for host galaxies of gamma-ray bursts by Millimetron (see Section 7.5) can shed light on this possibility.

8. Conclusion

To conclude, we can formulate three groups of unique tasks where Millimetron can play a decisive role and can significantly contribute to solving outstanding astrophysical, astrochemical, and cosmological issues.

(1) Studies of the vicinity of black holes and tests of general relativity. Studies of accretion flows and jets near the black hole horizons.

(2) Analysis of the interstellar medium and star formation. Studies of protostars, protoplanets, and protoplanetary discs, as well as of exoplanets and the Solar System. Studies of star formation conditions and of the interstellar medium enrichment by heavy elements.

(3) Formation and evolution of galaxies, studies of cosmological objects, and the development of the standard cosmological model.

Acknowledgements. The authors are deeply grateful to all whose comments were used in the preparation of this paper: V V Akimkin, A V Alakoz, A A Andrianov, N A Arkhipova, V S Beskin, M V Barkov, O V Verkhodanov, A A Volnova, Yu N Gnedin, T de Graauw, V K Dubrovich, A A Ermash, D E Ionov, N R Ikhsanov, P V Kaygorodov, S V Kalensky, A V Kasparova, M S Kirsanova, Yu Yu Kovalev, S G Moiseenko, Y N Pavlyuchenko, K A Postnov, M V Popov, O K Sil'chenko, V N Rudenko, A V Stepanov, S A Tyulbashev, M S Hramtsova, N N Shakhvorostova, A A Shatsky, B M Shustov, S V Chernov, as well as the staff of the P N Lebedev Physical Institute RAS (LPI), the P K Sternberg State Astronomical Institute (SAI MSU), the Institute of Astronomy RAS, the Main Astronomical Observatory RAS, the Pushchino Radio Astronomy Observatory and the Astro Space Center (ASC) LPI, which assisted in the preparation of the scientific program. The ASC LPI staff (N S Kardashev, I D Novikov, V N Lukash, S V Pilipenko, E V Mikheeva, A G Doroshkevich, P B Ivanov, V I Kostenko, T I Larchenkova, S F Likhachev, A V Smirnov) thanks L N Likhachova for the support. A G Doroshkevich, P B Ivanov, T I Larchenkova, V N Lukash, E V Miheeva, I D Novikov, S V Pilipenko

acknowledge the support from a grant from the President of the Russian Federation for State Support of Leading Scientific Schools NSH-4235.2014.2, the program DPS RAS OFN-17 "Active processes in galactic and extragalactic objects" and the program of the Presidium of the Russian Academy of Sciences P-21 "Nonstationary phenomena in objects of the Universe." D V Bisikalo and D S Wiebe are supported by a grant from the President of the Russian Federation for State Support of Leading Scientific Schools NSH-3620.2014.2. Yu A Schekinov is supported by the RFBR grant 12-02-00917-a. The work of I F Malov and V M Malofeev is supported by the RFBR grant 12-02-00661 and by the Presidium of the Russian Academy of Sciences (program "The origin, structure, and evolution of objects of the Universe"). A S Pozanenko is supported by the RFBR grants 12-02-01336, 13-01-92204, and 14-02-10015. The work of I D Novikov is supported by the RFBR grant 12-02-00276a. The work of I I Zinchenko is partially supported by a grant under the agreement between the Ministry of Education and Science of the Russian Federation and Nizhny Novgorod State University 02.V.49.21.0003 of 27 August 2013, as well as by the RFBR grant 13-02-12220-ofi_m. A M Sobolev's work was performed in the framework of the State Ministry of Education and Science of the Russian Federation (project 3.1781.2014/K). A M Cherepashchuk acknowledges the grant from the President of the Russian Federation for State Support of Leading Scientific Schools NSH-1675.2014.2 and the RFBR grant 14-02-00825.

References

1. Dole H et al. *Astron. Astrophys.* **451** 417 (2006)
2. Smirnov A V et al. *Proc. SPIE* **8442** 84424C (2012)
3. Krabbe A, Röser H P, in *Astronomical Instruments and Methods at the Turn of the 21st Century* (Reviews in Modern Astronomy, Vol. 12, Ed. R E Schielicke) (Hamburg: Astronomische Gesellschaft, 1999) p. 107; Krabbe A, Titz R, Röser H-P *Sterne Weltraum* **38** 1052 (1999)
4. Crill B P et al. *Astrophys. J. Suppl.* **148** 527 (2003)
5. Hoogeveen R W M et al. *Proc. SPIE* **5152** 347 (2004)
6. Pilbratt G L *Proc. SPIE* **4850** 586 (2003)
7. Kardashev N S et al. *Trudy Fiz. Inst. Ross. Akad. Nauk* **228** 112 (2000)
8. Wild W et al. *Exp. Astron.* **23** 221 (2009)
9. Kiuchi H "ALMA Memo. Coherence estimation on the measured phase noise in Allan standard deviation" (2005), http://legacy.nrao.edu/alma/memos/html-memos/alma530/memo530.pdf
10. Nakagawa T *Proc. SPIE* **7731** 77310O (2010)
11. Doeleman S S et al. *Nature* **455** 78 (2008)
12. McKee C F, Ostriker E C *Annu. Rev. Astron. Astrophys.* **45** 565 (2007)
13. Goicoechea J R, Cernicharo J *Astrophys. J.* **554** L213 (2001)
14. Ade P A R et al. (Planck Collab.) *Astron. Astrophys.* **536** A19 (2011)
15. Roberge W, Dalgarno A *Astrophys. J.* **255** 489 (1982)
16. Cecchi-Pestellini C, Dalgarno A *Astrophys. J.* **413** 611 (1993)
17. Voshchinnikov N V (2014), private communication
18. Efremov Yu N *Mon. Not. R. Astron. Soc.* **405** 1531 (2010)
19. Fukui Y, Kawamura A *Annu. Rev. Astron. Astrophys.* **48** 547 (2010)
20. Fukui Y et al. *Astrophys. J.* **780** 36 (2014)
21. Inutsuka S-I, Koyama H *Astrophys. Space Sci.* **281** 67 (2002)
22. Khoperskov S A et al. *Mon. Not. R. Astron. Soc.* **428** 2311 (2013)
23. Pineda J L et al. *Astron. Astrophys.* **554** 103 (2013)
24. Kirsanova M S et al. *Mon. Not. R. Astron. Soc.* **388** 729 (2008)
25. Kirsanova M S et al. *Mon. Not. R. Astron. Soc.* **437** 1593 (2014)
26. Crockett N R et al. *Astron. Astrophys.* **521** L21 (2010)
27. http://www.sron.rug.nl/millimetron/OxygenPuzzle
28. Walmsley M, van der Tak F, in *Proc. of the Dusty and Molecular Universe: a Prelude to Herschel and ALMA, 27–29 October 2004, Paris, France* (ESA SP-577, Ed. A Wilson) (Noordwijk: ESA Publ. Division, 2005) p. 55
29. Wyrowski F at al. *Astron. Astrophys.* **542** L15 (2012)
30. Kirsanova M S, Wiebe D S, Sobolev A M *Astron. Rep.* **53** 611 (2009); *Astron. Zh.* **86** 661 (2009)
31. Bergin E A et al. *Nature* **493** 644 (2013)
32. Bergin E A et al. *Astron. Astrophys.* **521** L33 (2010)
33. Hogerheijde M R et al. *Science* **334** 338 (2011)
34. Lahuis F et al. *Astrophys. J* **636** L145 (2006)
35. Akimkin V et al. *Astrophys. J.* **766** 8 (2013)
36. Akimkin V et al. *Astrophys. Space Sci.* **335** 33 (2011)
37. Young Ch H et al. *Astrophys. J. Suppl.* **154** 396 (2004)
38. Pavlyuchenkov Ya N, Wiebe D S, Fateeva A M, Vasyunina T S *Astron. Rep.* **55** 1 (2011); *Astron. Zh.* **88** 3 (2011)
39. Robitaille Th O et al. *Astrophys. J. Suppl.* **167** 256 (2006)
40. Robitaille Th P et al. *Astrophys. J. Suppl.* **169** 328 (2007)
41. Zinchenko I I (2014), in preparation
42. Henning Th et al. *Astron. Astrophys.* **518** L95 (2010)
43. Müller T G et al. *Astron. Astrophys.* **566** A22 (2014); arXiv: 1404.5847
44. Gray M *Maser Sources in Astrophysics* (Cambridge: Cambridge Univ. Press, 2012)
45. Sobolev A M et al. *Proc. Int. Astron. Union* **242** 81 (2007)
46. Moran J M et al. *Proc. Int. Astron. Union* **242** 391 (2007)
47. Parfenov S Yu, Sobolev A M *Mon. Not. R. Astron. Soc.* **444** 620 (2014)
48. Zhilkin A G, Bisikalo D V, Boyarchuk A A *Phys. Usp.* **55** 115 (2012); *Usp. Fiz. Nauk* **182** 121 (2012)
49. Matveyenko L I et al. *Astron. Lett.* **30** 100 (2004); *Pis'ma Astron. Zh.* **30** 121 (2004)
50. Sobolev A M et al. *Science* (2014), in print
51. Fridman A M, Bisikalo D V *Phys. Usp.* **51** 551 (2008); *Usp. Fiz. Nauk* **178** 577 (2008)
52. Kurbatov E P, Bisikalo D V, Kaygorodov P V *Phys. Usp.* **57** 787 (2014); *Usp. Fiz. Nauk* **184** 851 (2014)
53. Seager S *Exoplanet Atmospheres: Physical Processes* (Princeton, N.J.: Princeton Univ. Press, 2010)
54. Vidal-Madjar A et al. *Nature* **422** 143 (2003)
55. Linsky J et al. *Astrophys. J.* **717** 1291 (2010)
56. France K et al. *Astrophys. J.* **712** 1277 (2010)
57. Fossati L et al. *Astrophys. J.* **714** L222 (2010)
58. Narita N et al. *Astrophys. J.* **773** 144 (2013)
59. Mayer A et al. *Astron. Astrophys.* **549** A69 (2013)
60. Decin L *Adv. Space Res.* **50** 843 (2012)
61. Justtanont K et al. *Astron. Astrophys.* **537** 144 (2012)
62. Cernicharo J et al. *Astrophys. J.* **778** L25 (2013)
63. Ueta T et al. *Astron. Astrophys.* **565** A36 (2014)
64. Kardashev N S *Nature* **278** 28 (1979)
65. Mauersberger R et al. *Astron. Astrophys.* **306** 141 (1996)
66. Dyson F *Science* **131** 1667 (1960)
67. Slysh V I, in *The Search for Extraterrestrial Life — Recent Developments: Proc. of the 112th Symp. of the Intern. Astronomical Union, Boston, Mass., USA, June 18–21, 1984* (Ed M D Papagiannis) (Dordrecht: D. Reidel, 1985) p. 315
68. Carrigan R *Astrophys. J.* **698** 2075 (2009)
69. Kilic M et al. *Astrophys. J.* **678** 1298 (2008)
70. Farihi J et al. *Mon. Not. R. Astron. Soc.* **432** 1955 (2013)
71. Cutri R M et al. "WISE All-sky Data Release", 2012yCat.2311....0C (2012)
72. Kawka A, Vennes S *Mon. Not. R. Astron. Soc. Lett.* **439** L90 (2014)
73. Malofeev V et al. *Astron. Astrophys.* **285** 201 (1994)
74. Xilouris K M et al. *Astron. Astrophys.* **288** L17 (1994)
75. Morris D et al. *Astron. Astrophys.* **322** L17 (1997)
76. Löhmer O et al. *Astron. Astrophys.* **480** 623 (2008)
77. Kramer M et al. *Astrophys. J.* **488** 364 (1997)
78. Camilo F et al. *Astrophys. J.* **669** 561 (2007)
79. Camilo F et al. *Astrophys. J.* **679** 681 (2008)
80. Malov I F *Astron. Rep.* **41** 617 (1997); *Astron. Zh.* **76** 542 (1997)
81. Malov I F *Astron. Rep.* **58** 139 (2014); *Astron. Zh.* **91** 194 (2014)
82. Popov M V et al. *Astrophys. J. Lett.* (2014), in print
83. Heger A et al. *Astrophys. J.* **591** 288 (2003)
84. Marscher A P et al. *Astrophys. J.* **763** L15 (2013)
85. Mackey A D et al. *Mon. Not. R. Astron. Soc.* **386** 65 (2008)

86. Strader J et al. *Nature* **490** 71 (2012)
87. Chomiuk L et al. *Astrophys. J.* **777** 69 (2013); arXiv:1306.6624
88. Fabbiano G *Annu. Rev. Astron. Astrophys.* **27** 87 (1989)
89. Frank J, King A, Raine D J *Accretion Power in Astrophysics* (Cambridge: Cambridge Univ. Press, 2002)
90. Colbert E J M, Mushotzky R F *Astrophys. J.* **519** 89 (1999)
91. Liu J-F, Bregman J N *Astrophys. J. Suppl.* **157** 59 (2005)
92. Liu Q Z, Mirabel I F *Astron. Astrophys.* **429** 1125 (2005)
93. Colbert E J M, Ptak A F *Astrophys. J. Suppl.* **143** 25 (2002)
94. Swartz D A *ASP Conf. Ser.* **423** 277 (2010)
95. Mushotzky R *Prog. Theor. Phys. Suppl.* **155** 27 (2004)
96. Miller J M et al. *Astrophys. J. Lett.* **585** L37 (2003)
97. Poutanen J et al. *Mon. Not. R. Astron. Soc.* **377** 1187 (2007)
98. Kording E, Falcke H, Markoff S *Astron. Astrophys.* **382** L13 (2002)
99. Feng H, Soria R *New Astron. Rev.* **55** 166 (2011)
100. Miller M, Coleman H, Douglas P *Astrophys. J.* **576** 894 (2002)
101. Farrell S A et al. *Nature* **460** 73 (2009)
102. Webb N et al. *Science* **337** 554 (2012)
103. Miller N A, Mushotzky R F, Neff S G *Astrophys. J.* **623** L109 (2005)
104. Kaaret P et al. *Science* **299** 365 (2003)
105. Harrison F, in *Intern. Conf. ZELDOVICH-100, Moscow, Russia, 16–20 June 2014*
106. Bisnovatyi-Kogan G S *Sov. Astron.* **14** 652 (1971); *Astron. Zh.* **47** 813 (1970)
107. Moiseenko S G, Bisnovatyi-Kogan G S, Ardeljan N V *Mon. Not. R. Astron. Soc.* **370** 501 (2006)
108. Bisnovatyi-Kogan G S, Moiseenko S G, Ardelyan N V *Astron. Rep.* **52** 997 (2008); *Astron. Zh.* **85** 1109 (2008)
109. Bisnovatyi-Kogan G S, Moiseenko S G, Ardelyan N V *Astron. Rep.* **36** 285 (1992); *Astron. Zh.* **69** 563 (1992)
110. Barkov M V, Komissarov S S *Mon. Not. R. Astron. Soc.* **415** 944 (2011)
111. Chevalier R A *Astrophys. J. Lett.* **752** 2 (2012)
112. Taam R E, Sandquist E L *Astron. Astrophys.* **38** 113 (2000)
113. Field G B, Rogers R D *Astrophys. J.* **403** 94 (1993)
114. Kardashev N S *Mon. Not. R. Astron. Soc.* **276** 515 (1995)
115. Lobanov A P *Astron. Astrophys.* **330** 79 (1998)
116. Tyul'bashev S A *Astron. Astrophys.* **387** 818 (2002)
117. Eatough et al. *Nature* **501** 391 (2013)
118. Marrone et al. *Astrophys. J. Lett.* **654** 57 (2007)
119. Trippe et al. *Astron. Astrophys.* **540** A74 (2012)
120. Ivanov P B (2013), private communication
121. Dexter J et al. *Astrophys. J.* **717** 1092 (2010)
122. Lu Y et al. *Astrophys. J.* (2014), in print
123. Muller T, Frauendiener J *Eur. J. Phys.* **33** 955 (2012)
124. Komossa S, Bade N *Astron. Astrophys.* **343** 775 (1999)
125. Bloom J S et al. *GCN Circ.* (11847) 1 (2011)
126. Beskin V S *Phys. Usp.* **53** 1199 (2010); *Usp. Fiz. Nauk* **180** 1241 (2010)
127. Barkov M V, Komissarov S S *Mon. Not. R. Astron. Soc.* **401** 1644 (2010)
128. Barkov M V, Baushev A N *New Astron.* **16** 45 (2011)
129. McKinney J C, Uzdensky D A *Mon. Not. R. Astron. Soc.* **419** 573 (2012)
130. McKinney J C, Tchekhovskoy A, Blandford R D *Mon. Not. R. Astron. Soc.* **423** 3083 (2012)
131. De Bruyn A G *NFRA Note* **655** 1 (1996)
132. Brentjens M A, de Bruyn A G, in *Proc. of the Riddle of Cooling Flows in Galaxies and Clusters of Galaxies, Charlottesville, VA, USA, May 31–June 4, 2003* (Eds T H Reiprich, J C Kempner, N Soker) (Charlottesville, VA: Univ. of Virginia, 2004)
133. Vogt C, Dolag K, Enslin T A *Mon. Not. R. Astron. Soc.* **358** 726 (2005)
134. Brentjens M A, de Bruyn A G *Astron. Astrophys.* **441** 1217 (2005)
135. Aharonian F et al. *Astrophys. J.* **664** L71 (2007)
136. Begelman M C, Fabian A C, Rees M J *Mon. Not. R. Astron. Soc.* **384** L19 (2008)
137. Giannios D, Uzdensky D A, Begelman M C *Mon. Not. R. Astron. Soc.* **395** L29 (2009)
138. Barkov M V et al. *Mon. Not. R. Astron. Soc.* **749** 119 (2012)
139. Mesler R A, Pihlström Y M *Astrophys. J.* **774** 77 (2013)
140. Berger E et al. *Nature* **426** 154 (2003)
141. Frail D A et al. *Astrophys. J.* **619** 994 (2005)
142. Barkov M V, Pozanenko A S *Mon. Not. R. Astron. Soc.* **417** 2161 (2011)
143. Michalowski M, Hjorth J, Watson D *Astron. Astrophys.* **514** A67 (2010)
144. Pope A, Chary R R *Astrophys. J.* **715** L171 (2010)
145. Dayal P, Hirashita H, Ferrara A *Mon. Not. R. Astron. Soc.* **403** 620 (2010)
146. Pohlen M et al. *Astron. Astrophys.* **518** L72 (2010)
147. Fritz M et al. *Astron. Astrophys.* **516** 34 (2012)
148. Smith M W L et al. *Astrophys. J.* **756** 40 (2012)
149. Holwerda B W et al. *Astron. Astrophys.* **444** 101 (2005)
150. Holwerda B W et al. *Astron. Nachr.* **334** 268 (2013)
151. Magrini L et al. *Astron. Astrophys.* **535** 13 (2011)
152. Grenier I A, Casandjian J M, Terrier R *Science* **307** 1292 (2005)
153. Abramova O V, Zasov A V *Astron. Lett.* **38** 755 (2012); *Pis'ma Astron. Zh.* **38** 843 (2012)
154. Karachentsev I et al. *Mon. Not. R. Astron. Soc.* **415** L31 (2011)
155. Das M, Boone F, Viallefond F *Astron. Astrophys.* **523** 63 (2010)
156. Hinz J L et al. *Astrophys. J.* **663** 895 (2007)
157. Kasparova A V et al. *Mon. Not. R. Astron. Soc.* **437** 3072 (2014)
158. Xilouris E et al. *Astrophys. J.* **651** L107 (2006)
159. Temi P, Brighenti F, Mathews W G *Astrophys. J.* **660** 1215 (2007)
160. Agguirre A, Haiman Z *Astrophys. J.* **532** 28 (2000)
161. Johansson J, Morstell E *Mon. Not. R. Astron. Soc.* **426** 3360 (2012)
162. Nath B, Shchekinov Yu *Rep. Prog. Phys.* (2014), submitted
163. Polikarpova O L, Shchekinov Yu A *Astron. Zh.* (2014), in press
164. Chelouche D, Koester B P, Bowen D V *Astrophys. J.* **671** L97 (2007)
165. Muller S et al. *Astrophys. J.* **680** 975 (2008)
166. Menard B, Kilbinger M, Scranton R *Mon. Not. R. Astron. Soc.* **406** 1815 (2010)
167. McGee S L, Balogh M L *Mon. Not. R. Astron. Soc.* **405** 2069 (2010)
168. Kitayama T et al. *Astrophys. J.* **695** 1191 (2009)
169. Grossi M et al. *Astron. Astrophys.* **518** L52 (2010)
170. Baes M et al. *Astron. Astrophys.* **518** L53 (2010)
171. Simcoe R A et al. *Astrophys. J.* **637** 648 (2006)
172. Tumlinson J et al. *Science* **334** 948 (2011)
173. Vasiliev E O, Nath B B, Shchekinov Yu *Mon. Not. R. Astron. Soc.* **446** 1703 (2015); arXiv:1401.5070
174. Khramtsova M S et al. *Mon. Not. R. Astron. Soc.* **431** 2006 (2013)
175. Contursi A et al. *Astron. Astrophys.* **549** 118 (2013)
176. Dedikov S Yu, Shchekinov Yu A *Astron. Rep.* **48** 9 (2004); *Astron. Zh.* **81** 11 (2004)
177. Vasiliev E O, Dedikov S Yu, Shchekinov Yu A *Astrophys. Bull.* **64** 317 (2009); *Astrofiz. Byull.* **64** 333 (2009)
178. Shchekinov Yu A, Vasiliev E O *Astrophys. Space Sci.* (2014), submitted
179. Diaz-Santos T et al. *Astrophys. J. Lett.* **788** L17 (2014)
180. Kreckel K et al. *Astrophys. J.* **790** 26 (2014)
181. Satterfield T J et al. *Astron. J.* **144** 27 (2012)
182. Heiles C, Reach W T, Koo B-C *Astrophys. J.* **466** 191 (1996)
183. Tenorio-Tagle G *Astron. J.* **111** 1641 (1996)
184. Lemasle B et al. *Astron. Astrophys.* **558** 31 (2013)
185. Esteban C et al. *Mon. Not. R. Astron. Soc.* **433** 382 (2013)
186. Esteban C et al. *Mon. Not. R. Astron. Soc.* **443** 624 (2014)
187. Maiolino R et al. *Nature* **431** 533 (2004)
188. Gomez H L et al. *Astrophys. J.* **760** 96 (2012)
189. Gomez H L et al. *Mon. Not. R. Astron. Soc.* **420** 3557 (2012)
190. Krause O et al. *Nature* **432** 596 (2004)
191. Barlow M J et al. *Astron. Astrophys.* **518** L138 (2010)
192. Lagache G, Puget J-L, Dole H *Annu. Rev. Astron. Astrophys.* **43** 727 (2005)
193. Vieira J D et al. *Astrophys. J.* **719** 763 (2010)
194. Vieira J D et al. *Nature* **495** 344 (2013); arXiv:1303.2723
195. Blain A W *Mon. Not. R. Astron. Soc.* **283** 1340 (1996)
196. Negrello M et al. *Mon. Not. R. Astron. Soc.* **377** 1557 (2007)
197. Mao S D, Kochanek C S *Mon. Not. R. Astron. Soc.* **268** 569 (1994)
198. McLeod K K, Bechtold J *Astrophys. J.* **704** 415 (2009)
199. Irwin M J et al. *Astrophys. J.* **505** 529 (1998)
200. Vegetti S et al. *Nature* **481** 341 (2012)
201. Hezaveh Y D et al. *Astrophys. J.* **761** 20 (2012)
202. Viero M P et al. *Astrophys. J.* **772** 77 (2013)
203. Lukash V N, Mikheeva E V *Fizicheskaya Kosmologiya* (Physical Cosmology) (Moscow: Fizmatlit, 2010)

204. Lukash V N, Mikheeva E V, Malinovsky A M *Phys. Usp.* **54** 983 (2011); *Usp. Fiz. Nauk* **181** 1017 (2011)
205. Braatz R et al. *Astrophys. J.* **767** 154 (2013)
206. Galli D, Palla F *Annu. Rev. Astron. Astrophys.* **51** 163 (2013)
207. Shchekinov Yu A *Sov. Astron. Lett.* **12** 211 (1986); *Pis'ma Asron. Zh.* **12** 499 (1986)
208. Kamaya H, Silk J *Mon. Not. R. Astron. Soc.* **332** 251 (2009)
209. Becker R H et al. *Astron. J.* **122** 2850 (2001)
210. Dunkley J et al. *Astrophys. J. Suppl.* **180** 306 (2009)
211. Doroshkevich A G, Pilipenko S V *Astron. Rep.* **55** 567 (2011); *Astron. Zh.* **88** 617 (2011)
212. Dubrovich V K, Bajkova A, Khaikin V B *New Astron.* **13** 28 (2008)
213. Dubrovich V K, Lipovka A A *Astron. Astrophys.* **296** 307 (1995)
214. Zinchenko I, Dubrovich V, Henkel C *Mon. Not. R. Astron. Soc.* **415** L78 (2011)
215. de Bernardis P et al. *Astron. Astrophys.* **538** 86 (2012)
216. Zeldovich Ya B, Sunyaev R A *Astrophys. Space Sci.* **288** 4 (1969)
217. Zeldovich Ya B, Sunyaev R A *Astrophys. Space Sci.* **20** 9 (1969)
218. Sari R, Piran T, Narayan R *Astrophys. J.* **497** L17 (1998)
219. De Ugarte Postigo et al. *Astron. Astrophys.* **538** 44 (2012)
220. Perley D A et al. *Astrophys. J.* **781** 37 (2014)
221. Trenti M et al. *Astrophys. J. Lett.* **749** L38 (2012)
222. Tanvir N R et al. *Astrophys. J.* **754** 46 (2012)
223. Cucchiara A et al. *Astrophys. J.* **736** 7 (2011)
224. Bromm V, Coppi P S, Larson R B *Astron. J.* **564** 23 (2002)
225. Komissarov S S, Barkov M V *Mon. Not. R. Astron. Soc.* **402** L25 (2010)
226. Jakobsson P et al. *Astrophys. J.* **617** L21 (2004)
227. Thoene C C et al. *Mon. Not. R. Astron. Soc.* **428** 3590 (2013)
228. Castro-Tirado A J et al. *Astron. Astrophys.* **475** 101 (2007)
229. Perley D A et al. *Astron. J.* **138** 1690 (2009)
230. Zauderer B A et al. *Astrophys. J.* **767** 161 (2013)
231. Volnova A A et al. *Mon. Not. R. Astron. Soc.* **442** 2586 (2014)
232. Linde A *Particle Physics and Inflationary Cosmology* (Chur: Harwood Acad. Publ., 1990)
233. Linde A, in *Universe or Multiverse*? (Ed. B Carr) (Cambridge: Cambridge Univ. Press, 2007) p. 127
234. Mukhanov V F *Physical Foundations of Cosmology* (Cambridge: Cambridge Univ. Press, 2007)
235. Smolin L *The Life of the Cosmos* (Oxford: Oxford Univ. Press, 1999)
236. Lukash V N, Mikheeva E V, Strokov V N *Phys. Usp.* **55** 831 (2012); *Usp. Fiz. Nauk* **182** 894 (2012)
237. Lukash V N, Mikheeva E V, Strokov V N *Phys. Usp.* **55** 204 (2012); *Usp. Fiz. Nauk* **182** 216 (2012)
238. Garay I, Robles-Pérez S *Int. J. Mod. Phys. D* **23** 1450043 (2014)
239. Nadezhin D K, Novikov I D, Polnarev A G *Sov. Astron.* **22** 129 (1978); *Astron. Zh.* **55** 216 (1978)
240. Carr B J et al. *Phys. Rev. D* **81** 104019 (2010)
241. Kardashev N S, Novikov I D, Shatskii A A *Astron. Rep.* **50** 601 (2006); *Astron. Zh.* **83** 675 (2006)
242. Doroshkevich A G, Kardashev N S, Novikov D I, Novikov I D *Astron. Rep.* **52** 616 (2008); *Astron. Zh.* **85** 685 (2008)
243. Pozanenko A, Shatskiy A *Gravit. Cosmol.* **16** 259 (2010); arXiv: 1007.3620
244. Shatskii A A, Novikov I D, Kardashev N S *Phys. Usp.* **51** 457 (2008); *Usp. Fiz. Nauk* **178** 481 (2008)
245. Novikov I D, Kardashev N S, Shatskii A A *Phys. Usp.* **50** 965 (2007); *Usp. Fiz. Nauk* **177** 1017 (2007)
246. Shatskii A A *Phys. Usp.* **52** 811 (2009); *Usp. Fiz. Nauk* **179** 861 (2009)
247. Novikov I D *Sov. Astron.* **8** 857 (1965); *Astron. Zh.* **41** 1075 (1964)
248. Novikov I D, Frolov V P *Physics of Black Holes* (Dordrecht: Kluwer Acad., 1989); Translated from Russian: *Fisika Chernykh Dyr* (Moscow: Nauka, 1986)
249. Retter A, Heller S *New Astron.* **17** 73 (2012)